Shape optimisation with the level set method for contact problems in linearised elasticity

Aymeric Maury, Grégoire Allaire, François Jouve

Shape optimisation with the level set method for contact problems in linearised elasticity

Aymeric Maury[1], Grégoire Allaire[2] and François Jouve[1]

[1]Laboratoire J.L. Lions (UMR CNRS 7598), University Paris Diderot, Paris, France
[2]CMAP (UMR CNRS 7641), Ecole Polytechnique, Palaiseau, France

Abstract

This article is devoted to shape optimisation of contact problems in linearised elasticity, thanks to the level set method. We circumvent the shape non-differentiability, due to the contact boundary conditions, by using penalised and regularised versions of the mechanical problem. This approach is applied to five different contact models: the frictionless model, the Tresca model, the Coulomb model, the normal compliance model and the Norton-Hoff model. We consider two types of optimisation problems in our applications: first, we minimise volume under a compliance constraint, second, we optimise the normal force, with a volume constraint, which is useful to design compliant mechanisms. To illustrate the validity of the method, 2D and 3D examples are performed, the 3D examples being computed with an industrial software.

1 Introduction

We study the shape optimisation of a structure, the behaviour of which is modeled by the equations of the linearised elasticity with unilateral contact boundary conditions and friction conditions. From an industrial point of view, these kinds of boundary conditions are of great interest, as they enable a more detailed and accurate modelisation of boundary conditions, compared to clamped or Dirichlet boundary conditions. From a mathematical point of view, they tend to make the whole optimisation more intricate. Indeed the mechanical problem takes the form of a variational inequation and, thus, is highly nonlinear. The study of the existence and uniqueness of a solution for frictionless contact and its regularity were performed, for instance, in [14], [8], more recently in [4] and, thanks to the use of pseudo-differential operators, in [50]. Similar results on frictionless auto-contact and auto-contact with Tresca friction can also be found in [37]. However, as soon as a more realistic friction model is taken into consideration, results on existence and uniqueness become harder to obtain [15], [35].

On the other hand, the shape optimisation of such problems presents the same difficulties as encountered in control theory of variational inequalities. As pointed out in [41] and [54], the frictionless contact solution can be written under the form of a projection onto a convex set, which is not differentiable in the usual sense but merely admits a so-called conical derivative [41]. Nevertheless, Mignot [41] managed to derive optimality conditions, thanks to this weak notion of differentiability. Using the conical derivative and writing the problem under a discretised form, Kocvara and al. [46] used a bundle algorithm to perform shape optimisation. Another way to get optimality conditions, see [5] and [3], is to introduce a regularised problem, depending on a small regularisation parameter, study its optimality conditions and pass to the limit when the regularisation parameter tends to zero. This approach, called penalisation, was used in numerical shape optimisation, for example in [12] using SIMP method, [48] and [32], using splines to parameterise the shape. Its convergence to the exact solution was proved in [13]. Another similar approach is the regularisation of the unilateral boundary conditions which was used in [56] and [55] in the context of SIMP method. Some authors, as in [58] and [29], write a saddle point formulation of the problem and use the so-called Lagrangian method, ignoring the non differentiability of the Lagrange multipliers arising in this formulation. Of course, it is possible to perform optimisation without derivatives, as in [10], using genetic algorithms, but the price to pay is the very large number of required iterations. As far as theoretical results are concerned, we refer to [24], [25], [21], [23] where,

for a particular optimisation problem, existence of an optimum is proved under assumptions of uniform Lipschitz regularity of the boundary, first proving the result for a discretisation, then passing to the continuous limit.

When friction comes into play, the shape differentiation becomes even more difficult. In [54], for the Tresca model (also called the prescribed friction model), a conical derivative is found out, merely in two-space dimensions and for specific directions of differentiation. Once again, penalised and regularised formulations can be used as in [31], [3] and [57]. Theoretical results are also given for normal compliance model in [35] and [36] and for Coulomb friction model in [22]. For this last model of friction, the uniqueness of the contact solution is not ensured for the continuous model and examples of non uniqueness can be built. Consequently, in [6] and [7], the authors analyse the derivation of the discretised problem, which admits a unique solution for small friction coefficients, by using subgradient calculus. Eventually, a thorough review of other results in shape optimisation for contact problems can be found in [28].

In this paper, we are interested in applying the levelset method for shape optimisation [2] to contact problems, possibly including friction. To the best of our knowledge, this is the first time that this method is used for shape optimisation of contact problems. We investigate four types of friction, one of them being the Norton Hoff model which has not been previously used in shape optimisation. The general and classical idea adopted here is to use the penalised and regularised formulations to compute derivatives, which avoids us to deal with intricate conical derivatives. We also tackle the issue of optimising some objectives depending on the normal force, a goal which was at the center of [34] and [10] but treated in a completely different way. This type of objective functions is useful to design compliant mechanisms, for example.

Section 2 presents the frictionless contact model and gives four different friction conditions depending on the chosen model: Tresca, Coulomb, Norton Hoff and normal compliance model. For each of them, we recall an existence result for its solution. Section 3 focuses on how to regularise these problems in order to easily compute derivatives of their solution with respect to the shape. We choose to penalise the normal condition and to regularise the tangential ones which will enable us to compute shape derivatives. The section ends with a short analysis of existence results of these new formulations. In Section 4, a general shape optimisation problem is introduced and shape derivatives are calculated using the adjoint method. Criteria used in the numerical examples are also proposed, especially criteria depending on the normal force. Section 5 briefly recalls the main ideas of the level set method for shape optimisation. Our numerical results are collected in Section 6. A large range of examples show the good performances of our approach and we did not observe a high sensitivity of the optimised solutions to the regularisation and penalisation parameters. The 2D cases are performed with the Scilab free software [51], while the 3D examples are computed using the finite element software SYSTUS from ESI-Group [16]. Eventually we conclude and give some perspectives in Section 7.

2 Contact models in linearised elasticity

In this paper Ω denotes an open bounded subset of $\mathbb{R}^d$ where $d = 2$ or 3 and represents the shape of the structure we want to optimise. Its boundary is divided into five disjoint parts meaning that:

$$\partial\Omega = \Gamma_0 \cup \Gamma_N \cup \Gamma_c \cup \Gamma \cup S.$$

The structure Ω is full of a linear isotropic elastic material with a Hooke's law charaterised by A, for any τ symmetric matrix, as:

$$A\tau = 2\mu\tau + \lambda Tr(\tau) I_d$$

where μ and λ are the Lamé moduli. On Γ_0, the structure is clamped and on Γ_N a force is applied. The free part of the boundary is Γ and the parts where contact conditions are enforced are S and Γ_c. Γ_c modelises a contact with an undeformable body, whereas S is an auto-contact part (as for instance a crack could be). So S lies in the interior of $\overline{\Omega}$, see Figure 1. We assume that $\Omega \cup S$ is smooth.

The displacement field u is then solution of the linearised elasticity system:

$$\begin{cases} -\operatorname{div}(Ae(u)) = f & \text{in } \Omega \\ u = 0 & \text{on } \Gamma_0 \\ Ae(u)n = g & \text{on } \Gamma_N \\ Ae(u)n = 0 & \text{on } \Gamma, \end{cases} \tag{1}$$

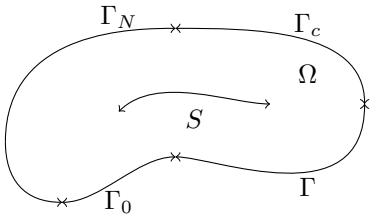

Figure 1: The open set Ω and its boundaries.

complemented with contact boundary conditions on Γ_c and S, which depend on the type of contact model we use. In (1), n denotes the exterior unit normal. To specify the contact boundary conditions, we first introduce some notations. For a vector $v \in \mathbb{R}^d$, we denote by v_t its tangential part:

$$v_t = v - (v \cdot n)\, n.$$

We also note the jump through S of v, noting S_- and S_+ the two sides of S:

$$[v] = v_{|S_-} - v_{|S_+}\,.$$

2.1 Sliding Contact

Sliding contact assumes there is no friction, which means that $(Ae(u)n)_t = 0$ on Γ_c and $(Ae(u)n)_t = 0$ on S_- and S_+. For the normal part on Γ_c, three conditions are needed:

$$u \cdot n \leq 0 \tag{2}$$

which prevents the penetration,

$$Ae(u)n \cdot n \leq 0 \tag{3}$$

meaning that the normal force on the contact surface is always in the sense opposite to the outward normal and the complementarity condition

$$(u \cdot n)(Ae(u)n \cdot n) = 0 \tag{4}$$

imposes either a contact: $(u \cdot n) = 0$ either, when there is no contact, a no force condition on Γ_c: $(Ae(u)n \cdot n) = 0$.

Concerning the normal part on S, the conditions are similar in terms of jumps:

$$\begin{cases} [u] \cdot n_- \leq 0 \\ Ae(u_{|S_-})n_- \cdot n_- = Ae(u_{|S_+})n_- \cdot n_- \leq 0 \\ ([u] \cdot n_-)(Ae(u_{|S_-})n_- \cdot n_-) = 0, \end{cases} \tag{5}$$

where n_- is the normal to S_- pointing toward S_+.

Coupling these boundary conditions with (1), the sliding contact problem can be written as:

$$\begin{cases} -\mathrm{div}(Ae(u)) &= f & \text{in } \Omega \\ u &= 0 & \text{on } \Gamma_0 \\ Ae(u)n &= g & \text{on } \Gamma_N \\ Ae(u)n &= 0 & \text{on } \Gamma \\ u \cdot n &\leq 0 & \text{on } \Gamma_c \\ Ae(u)n \cdot n &\leq 0 & \text{on } \Gamma_c \\ (u \cdot n)(Ae(u)n \cdot n) &= 0 & \text{on } \Gamma_c \\ [u] \cdot n_- &\leq 0 & \text{on } S \\ Ae(u_{|S_-})n_- \cdot n_- = Ae(u_{|S_+})n_- \cdot n_- &\leq 0 & \text{on } S \\ ([u] \cdot n_-)(Ae(u_{|S_-})n_- \cdot n_-) &= 0 & \text{on } S \\ (Ae(u)n)_t &= 0 & \text{on } \Gamma_c \cup S \end{cases} \tag{6}$$

Problem (6) can also be written as a variational inequation [14], where

$$K(\Omega) = \left\{ v \in H^1_{\Gamma_0}(\Omega)^d,\, v \cdot n \leq 0 \text{ on } \Gamma_c,\, [v] \cdot n_- \leq 0 \text{ on } S \right\}$$

is a closed convex set and $H^1_{\Gamma_0}(\Omega)^d = \left\{ v \in (H^1(\Omega))^d,\ v = 0 \text{ on } \Gamma_0 \right\}$:
find $u \in K(\Omega)$ such that

$$\int_\Omega Ae(u) : e(v-u)\, dx \geq \int_\Omega f \cdot (v-u)\, dx + \int_{\Gamma_N} g \cdot (v-u)\, ds \quad \forall v \in K(\Omega) \tag{7}$$

with $f \in L^2(\Omega)^d$ and $g \in L^2(\Gamma_N)^d$.

From (7) it follows that (6) is the Euler-Lagrange optimality condition of the minimisation problem:

$$u = \underset{v \in K(\Omega)}{\operatorname{argmin}} \frac{1}{2} \int_\Omega Ae(v) : e(v)\, dx - \int_\Omega f \cdot v\, dx - \int_{\Gamma_N} g \cdot v\, ds \tag{8}$$

which will be useful in the next section to penalise the problem.

The proof of existence and uniqueness of the solution u to (8) or (6) is a direct consequence of theorem 2.1 in [33] and Korn inequality (theorem 1.2.1 in [15] and theorem 3.1 in chapter 3 of [14]). It relies on the convexity of both $K(\Omega)$ and the quadratic energy functional.

2.2 Contact with friction

To add some friction conditions, it is necessary to change the tangential condition $(Ae(u)n)_t = 0$ on Γ_c and S. The most popular friction model is the Coulomb one, but we first state a simpler model derived from it and then present the different models which will be used in the shape optimisation part.

2.2.1 Tresca model

The Tresca friction model, also known as the model of given friction, was introduced in [14]. Even if it does not represent a realistic mechanical model, it can be used numerically to obtain the solution of the Coulomb friction model in a fixed point method and is mathematically well-posed. For the normal part (2), (3), (4) and (5) are kept. For the tangential part on Γ_c it is stated as:

$$\begin{aligned}
&\|(Ae(u)n)_t\| \leq \sigma_{\text{tr}} && \text{on } \Gamma_c \\
&\|(Ae(u)n)_t\| < \sigma_{\text{tr}} \Rightarrow u_t = 0 && \text{on } \Gamma_c \\
&\|(Ae(u)n)_t\| = \sigma_{\text{tr}} \Rightarrow \exists \lambda \geq 0,\, u_t = -\lambda (Ae(u)n)_t && \text{on } \Gamma_c
\end{aligned} \tag{9}$$

and on S:

$$\begin{aligned}
&(Ae(u)n)_t = (Ae(u_{|S_-})n_-)_t = -(Ae(u_{|S_+})n_+)_t && \text{on } S \\
&\|(Ae(u)n)_t\| \leq \sigma_{\text{tr}} && \text{on } S \\
&\|(Ae(u)n)_t\| < \sigma_{\text{tr}} \Rightarrow [u_t] = 0 && \text{on } S \\
&\|(Ae(u)n)_t\| = \sigma_{\text{tr}} \Rightarrow \exists \lambda \geq 0,\, [u_t] = -\lambda (Ae(u_{|S_-})n_-)_t && \text{on } S
\end{aligned}$$

where $\|\cdot\|$ denotes the classical euclidian norm on $\mathbb{R}^d$ and s is a smooth function representing the coefficient of friction. While the tangential force is smaller than the coefficient of friction, there is no sliding. If the tangential force reaches the threshold s, sliding can appear. This model is not well-suited to modelise real phenomena, since the tangential force does not take into account the normal force. Yet, like the problem (6), (9) can be written as a variational inequation and a minimisation problem of respectively the form: find $u \in K(\Omega)$ such that

$$\int_\Omega Ae(u) : e(v-u)\, dx + j_{\text{tr}}(v) - j_{\text{tr}}(u) \geq \int_\Omega f \cdot (v-u)\, dx + \int_{\Gamma_N} g \cdot (v-u)\, ds \ \ \forall v \in K(\Omega) \tag{10}$$

and

$$u = \underset{v \in K(\Omega)}{\operatorname{argmin}} \frac{1}{2} \int_\Omega Ae(v) : e(v)\, dx - \int_\Omega f \cdot v\, dx - \int_{\Gamma_N} g \cdot v\, ds + j_{\text{tr}}(v) \tag{11}$$

with

$$j_{\rm tr}(v) = \int_{\Gamma_c} \sigma_{\rm tr} \, \|v_t\| \, ds + \int_S \sigma_{\rm tr} \, \|[v]_t\| \, ds.$$

The proof of existence and uniqueness of the solution u of (11) is given in theorem 1.5.2 of [15]. Once again it relies on the convexity of the minimized functional.

2.2.2 Coulomb friction

The model of Coulomb friction is similar to the Tresca one, changing s into μ, a friction coefficient, times the norm of the normal force. For Γ_c:

$$\begin{aligned}
&\|(Ae(u)n)_t\| \leq \mu|(Ae(u)n\cdot n)| && \text{on } \Gamma_c\\
&\|(Ae(u)n)_t\| < \mu|(Ae(u)n\cdot n)| \Rightarrow u_t = 0 && \text{on } \Gamma_c\\
&\|(Ae(u)n)_t\| = \mu|(Ae(u)n\cdot n)| \Rightarrow \exists \lambda \geq 0,\ u_t = -\lambda (Ae(u)n)_t && \text{on } \Gamma_c
\end{aligned}$$

and for S:

$$\begin{aligned}
&(Ae(u)n)_t = (Ae(u_{|S_-})n_-)_t = -(Ae(u_{|S_+})n_+)_t && \text{on } S\\
&\|(Ae(u)n)_t\| \leq \mu|(Ae(u)n\cdot n)| && \text{on } S\\
&\|(Ae(u)n)_t\| < \mu|(Ae(u)n\cdot n)| \Rightarrow [u_t] = 0 && \text{on } S\\
&\|(Ae(u)n)_t\| = \mu|(Ae(u)n\cdot n)| \Rightarrow \exists \lambda \geq 0,\ [u_t] = -\lambda (Ae(u_{|S_-})n_-)_t && \text{on } S
\end{aligned}$$

For the normal part there is no change in the boundary conditions: (2), (3), (4) and (5). This can be written as the following variational inequation: find $u \in K(\Omega)$ such that

$$\int_\Omega Ae(u) : e(v-u)\, dx + j_{\rm co}(u,v) - j_{\rm co}(u,u) \geq \int_\Omega f\cdot(v-u)\, dx + \int_{\Gamma_N} g\cdot(v-u)\, ds \quad \forall v \in K(\Omega) \tag{12}$$

with

$$j_{\rm co}(u,v) = \int_{\Gamma_c} \mu|(Ae(u)n\cdot n)| \, \|v_t\| \, ds + \int_S \mu|(Ae(u)n\cdot n)| \, \|[v]_t\| \, ds.$$

which is a function of two variables.

This model is studied in chapters 1 and 3 of [15]. It is not equivalent to a minimisation problem. To our knowledge, there is no uniqueness results for this problem and the existence is only ensured for small friction coefficients. Yet the uniqueness was proven for the discretised problem in [20]. It is interesting, both for numerical [38] and theoretical [15] reasons, to note that this problem can be seen as the solution of a fixed point problem involving the solution of the Tresca model.

2.2.3 Norton-Hoff model

The Norton-Hoff model [42] is a variation of the previous friction model. The boundary condition is now a one-to-one relation between the tangential force and the tangential jump of the displacement (notwithstanding the normal force). It can be written as:

$$\begin{aligned}
&(Ae(u)n)_t = \mu|(Ae(u)n\cdot n)| \, \|u_t\|^{\rho-1} \, u_t && \text{on } \Gamma_c\\
&(Ae(u_{|S_-})n)_t = -(Ae(u_{|S_+})n)_t = -\mu|(Ae(u)n\cdot n)| \, \|[u_t]\|^{\rho-1} \, [u_t] && \text{on } S
\end{aligned} \tag{13}$$

where $0 < \rho < 1$. Adding the other boundary conditions (2), (3), (4) and (5), we obtain the following variational inequality. Find $u \in K(\Omega)$ such that

$$\int_\Omega Ae(u) : e(v-u)\, dx + j_{\rm nh}(u, v-u) \geq \int_\Omega f\cdot(v-u)\, dx + \int_{\Gamma_N} g\cdot(v-u)\, ds \quad \forall v \in K(\Omega) \tag{14}$$

where $j_{\rm nh}$ is a function of two variables, defined by

$$j_{\rm nh}(u,v) = \int_{\Gamma_c} \mu|(Ae(u)n\cdot n)| \, \|u_t\|^{\rho-1} \, u_t \cdot v_t \, ds + \int_S \mu|(Ae(u)n\cdot n)| \, \|[u]_t\|^{\rho-1} \, [u]_t \cdot [v]_t \, ds.$$

The one-to-one relation mentionned in (13) makes the model numerically simpler to solve than the Coulomb one. Let us remark that (14) is not equivalent to a minimisation problem.

2.2.4 Normal compliance model

The last friction model considered is the normal compliance model presented in [40] and studied in [35]. It is pretty similar to a problem where the normal inequality constraint is penalised with a small penalisation coefficient. On Γ_c it takes the following form:

$$\begin{aligned}
&(Ae(u)n\cdot n)n = -C_N(u\cdot n)_+^{m_N} n && \text{on } \Gamma_c\\
&\|(Ae(u)n)_t\| \le C_T(u\cdot n)_+^{m_T} && \text{on } \Gamma_c\\
&\|(Ae(u)n)_t\| < C_T(u\cdot n)_+^{m_T} \Rightarrow u_t = 0 && \text{on } \Gamma_c\\
&\|(Ae(u)n)_t\| = C_T(u\cdot n)_+^{m_T} \Rightarrow \exists\lambda\ge 0,\ u_t = -\lambda(Ae(u)n)_t && \text{on } \Gamma_c
\end{aligned} \tag{15}$$

and on S:

$$\begin{aligned}
&(Ae(u_{|S_-})n\cdot n)n_- = -(Ae(u_{|S_+})n\cdot n)n_- = -C_N([u]\cdot n_-)_+^{m_N} n && \text{on } S\\
&(Ae(u)n)_t = (Ae(u_{|S_-})n_-)_t = -(Ae(u_{|S_+})n_+)_t && \text{on } S\\
&\|(Ae(u)n)_t\| \le C_T([u]\cdot n_-)_+^{m_T} && \text{on } S\\
&\|(Ae(u)n)_t\| < C_T([u]\cdot n_-)_+^{m_T} \Rightarrow [u_t] = 0 && \text{on } S\\
&\|(Ae(u)n)_t\| = C_T([u]\cdot n_-)_+^{m_T} \Rightarrow \exists\lambda\ge 0,\ [u_t] = -\lambda(Ae(u_{|S_-})n_-)_t && \text{on } S
\end{aligned}$$

where $(\cdot)_+ = \max(0,\cdot)$, C_N and C_T are material coefficients and m_N and m_T are typically equal to 1 or 2 (see [35] for the possible value depending on the dimension d). Contrary to the other friction models, the normal part is different from the case of sliding contact. Again, it is possible to write a variational inequation equivalent to (15). Find $u\in K(\Omega)$ such that, for any $v\in H^1_{\Gamma_0}(\Omega)^d$,

$$\int_\Omega Ae(u):e(v-u)\,dx + j_{N,Nc}(u,v-u) + j_{T,Nc}(u,v) - j_{T,Nc}(u,u) \ge \int_\Omega f\cdot(v-u)\,dx + \int_{\Gamma_N} g\cdot(v-u)\,ds\,, \tag{16}$$

where

$$\begin{aligned}
j_{N,\mathrm{nc}}(u,v) &= \int_{\Gamma_c} C_N(u\cdot n)_+^{m_N} v\cdot n\,ds + \int_S C_N([u]\cdot n_-)_+^{m_N}[v]\cdot n\,ds\,,\\
j_{T,\mathrm{nc}}(u,v) &= \int_{\Gamma_c} C_T(u\cdot n)_+^{m_T}\,\|v_t\|\,ds + \int_S C_T([u]\cdot n_-)_+^{m_T}\,\|[v]_t\|\,ds.
\end{aligned}$$

This model allows interpenetration, which can represent a material loss at the surface of the material in contact. Existence and uniqueness results are given and discussed in [35] and [27] under smallness conditions on the coefficients C_N and C_T. Here again (16) is not equivalent to a minimisation problem.

3 Penalised and regularised formulations

As our goal is to optimise, thanks to a gradient algorithm, and therefore to compute the derivative of some functions depending on the displacement u, we need to investigate the differential properties of u with respect to the shape. Based on the work of [41], the authors of [54] have shown that the solution u of (7) admits at most a conical derivative because of the non differentiability of the projection map on closed convex sets in Hilbert spaces. We shall not define precisely what is a conical derivative (a type of "weak" multi-valued directional derivative). Let us simply say that it is quite difficult to use it in numerical practice since it requires a subgradient optimisation algorithm (see [46], for example, in finite dimension).

To avoid such intricate optimisation techniques, let us quickly investigate the different ways to numerically compute the solutions of problems described in Section 2. According to [17], there exist two main methods: the Lagrangian method and the penalisation method. The Lagrangian method introduces a Lagrange multiplier for the contact constraint, which will not be differentiable (basically for the same reasons preventing the solution u from being differentiable). The penalisation method has the nice property to transform inequations into equations and thus changes projection on closed convex sets into projection on linear spaces (in our cases $H^1_{\Gamma_0}(\Omega)$). In particular, for this penalisation approach, it is possible to differentiate these new equations. Consequently, we choose to study and use these penalised formulations.

In the different contact problems presented, there are two kinds of reasons which trigger the appearance of inequations. The first one, concerning the normal component of u on the boundary, is that u belongs to a convex set. This constraint will be penalised. The second one is the singularity in the tangential friction formulation due to the presence of the norm $\|\cdot\|$ which is not differentiable at zero. This term will be regularised, thanks to a regularisation of the norm $\|\cdot\|$.

3.1 Penalisation for the convex set

We now present the penalisation used to get rid of the constraint stating that the solution u is required to belong to $K(\Omega)$. This penalisation will be used for every model but the normal compliance one, and we explain how to add it to change the inequations into equations or other inequations. As a matter of fact, for problems involving friction, to get equations we also need to regularise the friction term (as said before). This is the reason why we only write the penalised equation associated with (11) in this subsection. For other models, they can be found in the next one.

To add the penalisation, the procedure differs whether the initial problem can be written as a minimisation problem, (11) and (8), or not, (12) and (14).

For (11) and (8), we change the functional to be minimised and the set of admissible solutions. Instead of minimising on $K(\Omega)$, we minimise on $H^1_{\Gamma_0}(\Omega)^d$. To approximate the condition $v\cdot n\leq 0$ on Γ_c and $[v]\cdot n_-\leq 0$ on S, we add to the functional a term of the form:

$$j_{N,\epsilon}(u)=\frac{1}{\epsilon}\left(\int_{\Gamma_c}\int_0^{u.n}\phi_\eta(t)\,dt\,ds+\int_S\int_0^{[u].n}\phi_\eta(t)\,dt\,ds\right) \tag{17}$$

where ϕ_η is a smooth function (at least C^1) meant to regularise $t\to t\mathcal{H}(t)$ with $\mathcal{H}$ the Heaviside function. For instance, taking a small parameter $\eta>0$:

$$\phi_\eta(x)=\begin{cases}0 & \text{for } x\in(-\infty;-\eta]\\ \dfrac{1}{4\eta}x^2+\dfrac{1}{2}x+\dfrac{\eta}{4} & \text{for } x\in[-\eta;\eta]\\ x & \text{for } x\in[\eta;+\infty).\end{cases} \tag{18}$$

We can then deduce a penalised variational formulation associated to (8):

$$\int_\Omega Ae(u):e(v)\,dx+j'_{N,\epsilon}(u,v)=\int_\Omega f\cdot v\,dx+\int_{\Gamma_N}g\cdot v\,ds.\ \ \forall v\in H^1_{\Gamma_0}(\Omega)^d, \tag{19}$$

where the directional derivative of (17) is

$$j'_{N,\epsilon}(u,v)=\frac{1}{\epsilon}\int_{\Gamma_c}\phi_\eta(u\cdot n)v\cdot n\,ds+\frac{1}{\epsilon}\int_S\phi_\eta([u]\cdot n_-)[v]\cdot n_-\,ds,$$

and an equivalent minimisation problem:

$$u=\underset{v\in H^1_{\Gamma_0}(\Omega)^d}{\operatorname{argmin}}\frac{1}{2}\int_\Omega Ae(v):e(v)\,dx-\int_\Omega f\cdot v\,dx-\int_{\Gamma_N}g\cdot v\,ds+j_{N,\epsilon}(v).$$

Problems (12) and (14) cannot be written as minimisation problems, therefore we need to work directly on the variational inequation. The idea is to add a term $j'_{N,\epsilon}(u,v-u)$ on the left hand side and change the spaces of the solutions as done in [15], chapter 3, keeping in mind that to get an equation we still need to regularise the friction term.

3.2 Regularisation of the friction term

In the friction models (10), (12), (14) and (16) we also need to regularise the norm $\|\cdot\|$ to transform inequations into equations. Let $\mathcal{N}_\eta$ be a smooth function (at least twice differentiable) approximating the norm. For instance, following [15]:

$$\mathcal{N}_\eta(x)=\begin{cases}\|x\| & \text{for } \|x\|\geq\eta,\\ -\dfrac{1}{8\eta^3}\|x\|^4+\dfrac{3}{4\eta}\|x\|^2+\dfrac{3}{8}\eta & \text{for } \|x\|\leq\eta.\end{cases}$$

The new penalised and regularised equations are then given as follows.

- For the Tresca model:

$$\int_\Omega Ae(u) : e(v)\,dx + j'_{\mathrm{tr},\eta}(u,v) + j'_{N,\epsilon}(u,v) = \int_\Omega f\cdot v\,dx + \int_{\Gamma_N} g\cdot v\,ds \quad \forall v \in H^1_{\Gamma_0}(\Omega)^d \tag{20}$$

  where $j'_{\mathrm{tr},\eta}(u,v)$ denotes the derivative of $j_{\mathrm{tr},\eta}$ at u in the direction v with

$$j_{\mathrm{tr},\eta}(v) = \int_{\Gamma_c} \sigma_{\mathrm{tr}}\mathcal{N}_\eta(v_t)\,ds + \int_S \sigma_{\mathrm{tr}}\mathcal{N}_\eta([v]_t)\,ds$$

  The penalised and regularised Tresca problem can be written as a minimisation problem:

$$u = \underset{v\in H^1_{\Gamma_0}(\Omega)^d}{\operatorname{argmin}} \frac{1}{2}\int_\Omega Ae(v) : e(v)\,dx - \int_\Omega f\cdot v\,dx - \int_{\Gamma_N} g\cdot v\,ds + j_{N,\epsilon}(v) + j_{\mathrm{tr},\eta}(v)$$

  It is not the case for the other friction models described in the sequel.

- For the Coulomb model:

$$\int_\Omega Ae(u) : e(v)\,dx + j'_{\mathrm{co},\epsilon,\eta}(u,v) + j'_{N,\epsilon}(u,v) = \int_\Omega f\cdot u\,dx + \int_{\Gamma_N} g\cdot u\,ds \quad \forall v \in H^1_{\Gamma_0}(\Omega)^d. \tag{21}$$

  where

$$j'_{\mathrm{co},\epsilon,\eta}(u,v) = \int_{\Gamma_c} \frac{\mu}{\epsilon}\phi_\eta(u\cdot n)\mathcal{N}'_\eta(u_t)\cdot v_t\,ds + \int_S \frac{\mu}{\epsilon}\phi_\eta([u]\cdot n_-)\mathcal{N}'_\eta([u]_t)\cdot[v]_t\,ds$$

  and $\mathcal{N}'_\eta$ is the derivative of $\mathcal{N}_\eta$.

- For the Norton-Hoff model:

$$\int_\Omega Ae(u) : e(v)\,dx + j_{\mathrm{nh},\epsilon,\eta}(u,v) + j'_{N,\epsilon}(u,v) = \int_\Omega f\cdot v\,dx + \int_{\Gamma_N} g\cdot v\,ds \quad \forall v \in H^1_{\Gamma_0}(\Omega)^d. \tag{22}$$

  where

$$j_{\mathrm{nh},\epsilon,\eta}(u,v) = \int_{\Gamma_c} \frac{\mu}{\epsilon}\phi_\eta(u\cdot n)\mathcal{N}_\eta(u_t)^{\rho-1}u_t\cdot v_t\,ds + \int_S \frac{\mu}{\epsilon}\phi_\eta([u]\cdot n_-)\mathcal{N}_\eta([u]_t)^{\rho-1}[u]_t\cdot[v]_t\,ds$$

- For the normal compliance model:

$$\int_\Omega Ae(u) : e(v)\,dx + j_{N,r,Nc}(u,v) + j'_{T,\eta,Nc}(u,v) = \int_\Omega f\cdot v\,dx + \int_{\Gamma_N} g\cdot v\,ds \quad \forall v \in H^1_{\Gamma_0}(\Omega)^d \tag{23}$$

  with

$$j_{N,\mathrm{nc,r}}(u,v) = \int_{\Gamma_c} C_N\phi_\eta(u\cdot n)^{m_N}v\cdot n\,ds + \int_S C_N\phi_\eta([u]\cdot n_-)^{m_N}[v]\cdot n\,ds,$$

$$j'_{T,\mathrm{nc},\eta}(u,v) = \int_{\Gamma_c} C_T\phi_\eta(u\cdot n)^{m_T}\mathcal{N}'_\eta(u_t)\cdot v_t\,ds + \int_S C_T\phi_\eta([u]\cdot n_-)^{m_T}\mathcal{N}'_\eta([u]_t)\cdot[v]_t\,ds.$$

  For this last model, both the normal and tangential terms were regularised but no penalisation is needed as the original equation is already posed in the whole space $H^1_{\Gamma_0}(\Omega)^d$.

We finally conclude that all regularised and penalised formulations (19), (20), (21), (22) and (23) can be written in full generality as nonlinear variational formulation: ind $u \in H^1_{\Gamma_0}(\Omega)^d$ such that,

$$\int_\Omega Ae(u) : e(u)\,dx + \int_{S\cup\Gamma_c} j(u,v,n)\,ds = \int_\Omega f\cdot v\,dx + \int_{\Gamma_N} g\cdot v\,ds \quad \forall v \in H^1_{\Gamma_0}(\Omega)^d, \tag{24}$$

where the integrand $j(u,v,n)$ is nonlinear with respect to the solution u but linear with respect to the test function v.

3.3 Differentiability of the penalised and regularised terms

The fact that ϕ_η, defined by (18), is smooth does not imply it is Fréchet differentiable from $L^2(\Gamma_c)$ to $L^2(\Gamma_c)$, see section 4.3 in [59]. It only implies the Gâteaux differentiability at each point $x \in \Gamma_c$. Nevertheless we can state the following lemma.

Lemma 3.3.1. *ϕ_η is differentiable from $H^{\frac{1}{2}}(\Gamma_c) \cap H^{\frac{1}{2}}(S)$ into $L^2(\Gamma_c) \cap L^2(S)$.*

Proof. This is an application of theorem 7 in [18]. We introduce the Nemytskij operator (associated with ϕ_η) $\Phi_\eta : u \to \phi_\eta(u)$ where $u \in L^p(\Gamma_c) \cap L^p(S)$ with p fixed later on. This theorem ensures its Fréchet differentiability from $L^p(\Gamma_c) \cap L^p(S)$ to $L^2(\Gamma_c) \cap L^2(S)$ if the following conditions are fulfilled:

- ϕ_η is a C^1 function from $\mathbb{R}$ to $\mathbb{R}$.
- The Nemytskij operator associated with ϕ'_η is continuous from $L^p(\Gamma_c) \cap L^p(S)$ to $L^r(\Gamma_c) \cap L^r(S)$ with $r = 2p/(p-2)$.

As $u \in H^{\frac{1}{2}}(\Gamma_c) \cap H^{\frac{1}{2}}(S)$, by Sobolev embeddings we deduce $u \in L^p(\Gamma_c) \cap L^p(S)$ with $p = 2(d-1)/(d-3/2)$. This means that $r = 4(d-1)$. It is clear that that $y \to \phi'_\eta(y)$ exists and is continuous (ϕ'_η is also globally Lipschitz continuous). Due to the choice of the penalisation, ϕ'_η is bounded (depending on the parameter of penalisation). Remark 4 in [18] then implies the continuity from $L^p(\Gamma_c) \cap L^p(S)$ to $L^r(\Gamma_c) \cap L^r(S)$ with $r = 2p/(p-2)$. □

Remark 3.3.1. *As $u \in H^1_{\Gamma_0}(\Omega)^d$, it follows that $u \cdot n \in H^{\frac{1}{2}}(\Gamma_c) \cap H^{\frac{1}{2}}(S)$ for Ω smooth enough. Then $u \to \phi_\eta(u \cdot n)$ is Fréchet differentiable from $H^1_{\Gamma_0}(\Omega)^d$ into $L^2(\Gamma_c) \cap L^2(S)$.*

Remark 3.3.2. *The regularisation term $\mathcal{N}_\eta$ is twice differentiable from $\mathbb{R}^d$ to $\mathbb{R}^d$. Moreover its derivative is bounded, so, thanks to theorem 8 in [18], it is Gâteaux differentiable from $L^2(\Gamma_c) \cap L^2(S)$ into $L^2(\Gamma_c) \cap L^2(S)$. As its second derivative is bounded by a linear function, it is also twice Fréchet differentiable from $H^{\frac{1}{2}}(\Gamma_c) \cap H^{\frac{1}{2}}(S)$ into $L^2(\Gamma_c) \cap L^2(S)$, thanks to theorem 7 in [18] applied two times. The proof is the same as in Lemma 3.3.1.*

3.4 Existence and uniqueness of the penalised/regularised formulation

For (19) and (20), existence and uniqueness results are easily proved by taking advantage of their respective minimisation problem formulation.

Theorem 3.4.1. *The problems (20) and (19) admit a unique solution $u \in H^1_{\Gamma_0}(\Omega)^d$, when $f \in L^2(\Omega)^d$, $g \in L^2(\Gamma_N)^d$, ϕ_η is positive increasing and $\mathcal{N}_\eta$ is convex positive.*

Proof. We introduce the functional:

$$E(u) = \frac{1}{2}a(u,u) + \frac{1}{\epsilon}\left(\int_{\Gamma_c}\int_0^{u.n} \phi_\eta(t)\,dt\,ds + \int_S \int_0^{[u].n} \phi_\eta(t)\,dt\,ds\right) + j_\eta(u) - \int_{\Gamma_N} g \cdot u\,ds - \int_\Omega f \cdot u\,dx$$

with $a(u,u) = \displaystyle\int_\Omega Ae(u) : e(u)\,dx$ and $j_\eta(u) = 0$ for (19) and $j_\eta(u) = \displaystyle\int_{\Gamma_c} \sigma_{\mathrm{tr}}\mathcal{N}_\eta(u_t)\,ds + \int_S \sigma_{\mathrm{tr}}\mathcal{N}_\eta([u]_t)\,ds$ for (20). Thanks to Korn inequality, $u \to a(u,u)$ is strictly convex. We now prove that $\psi : u \to \displaystyle\int_{\Gamma_c} \frac{1}{\epsilon}\int_0^{u.n} \phi_\eta(t)\,dt\,ds$ is convex. We compute the Hessian of ψ:

$$D^2\psi(u)(h,h') = \int_{\Gamma_c} \frac{1}{\epsilon}\phi'_\eta(u \cdot n)h' \cdot n\ h \cdot n\,ds$$

which is positive as ϕ'_η is positive. Moreover, since $\mathcal{N}_\eta$ is convex, j_η is convex, lower semi-continuous. So $u \to E(u)$ is strictly convex, lower semi-continuous on $H^1_{\Gamma_0}(\Omega)^d$. It is also bounded below as ϕ_η is non negative and an approximation of $x \to x\mathcal{H}(x)$ (for instance $\phi_\eta([u] \cdot n)$ vanishes when $[u] \cdot n$ is smaller than $-\eta$). It ensures the existence of a unique minimiser of E on $H^1_{\Gamma_0}(\Omega)^d$. To conclude we just need to remark that the optimality criterion is exactly (19) or (20), therefore both admit one and only one solution. □

We now turn to the other models. For (21) the existence is proved in chapter 3 of [15]. A proof similar to that for (21) can be done for (22). For these two cases, the uniqueness is not ensured. For the normal compliance model we refer to [19] for existence and uniqueness.

4 Optimisation problem

Our goal is to minimise a certain function $J(\Omega)$ depending on u, the displacement which solves one of the contact formulations given in section 2 under constraints also depending on u noted $C(\Omega)$:

$$\begin{cases} \min J(\Omega) \\ \Omega \in \mathcal{U}_{ad} \\ u \text{ solution of (24)} \\ C(\Omega) \leq 0 \end{cases} \tag{25}$$

where $\mathcal{U}_{ad}$ is the set of admissible shapes. These shapes should be included into a fixed domain D, $\Omega \subset D$, and the Dirichlet boundary $\Gamma_0 \subset \partial D$ is not allowed to change. In the following we denote Γ_m the part of the boundary of Ω which is allowed to change.

4.1 Shape derivative

To minimise (25) we apply a gradient method, therefore we need to compute derivatives with respect to Ω. We choose to use the notion introduced by Hadamard and then extensively studied, see for instance [26], [43], [49], [53] or [54]. Starting from a smooth domain Ω_0, the variation of the domain takes the form:

$$\Omega_\theta = (Id + \theta)(\Omega_0)$$

with $\theta \in W^{1,\infty}(\mathbb{R}^d, \mathbb{R}^d)$ and Id the identity map. When θ is sufficiently small, $Id+\theta$ is a diffeomorphism in $\mathbb{R}^d$, see [1]. Once the variation of the shape is defined, it is possible to define the notion of Gâteaux derivative for a function J depending on the shape.

Definition 4.1. *The shape derivative $J'(\Omega)(\theta)$ of $J(\Omega)$ at Ω in the direction θ is defined as the derivative at 0 of the application $t \to J((Id + t\theta)(\Omega))$ which means:*

$$J((Id + t\theta)(\Omega)) = J(\Omega) + tJ'(\Omega)(\theta) + o(t)$$

where $J'(\Omega)$ is a continuous linear form on $W^{1,\infty}(\mathbb{R}^d, \mathbb{R}^d)$.

We recall the following classical theorem [1] which will be used in the next section.

Theorem 4.1.1. *Let $\Omega \in \mathcal{U}_{ad}$ be a smooth open domain, ϕ a smooth function defined in $\mathbb{R}^d$,*

$$J_v(\Omega) = \int_\Omega \phi(x)\, dx \quad \text{and} \quad J_s(\Omega) = \int_{\partial\Omega} \phi(x)\, ds.$$

These two functions are shape differentiable at Ω in the direction $\theta \in W^{1,\infty}(\mathbb{R}, \mathbb{R})$ and

$$J'_v(\Omega)(\theta) = \int_{\partial\Omega} \theta \cdot n\phi\, ds \quad \text{and} \quad J'_s(\Omega)(\theta) = \int_{\partial\Omega} \theta \cdot n \left(\frac{\partial\phi}{\partial n} + H\phi\right) ds$$

where $H = \operatorname{div}(n)$ is the mean curvature of $\partial\Omega$.

We also give the shape derivative of the normal (see proposition 5.4.14 in [26]).

Proposition 4.1.1. *Let Ω be a C^2 domain and $n \in C^1(\mathbb{R}^d, \mathbb{R}^d)$ an extension of the unit normal to $\partial\Omega$. Denote $\Omega_{t\theta} = \Phi(t)\Omega_0$ with $\Phi(t) = (Id + t\theta)$. Then:*

$$t \to n_t = \frac{w(t)}{\|w(t)\|} \text{ with } w(t) = (\nabla^T \Phi(t)^{-1} n) \circ \Phi(t)^{-1}$$

is an extension to the normal of $\partial\Omega_{t\theta}$, is differentiable in 0 and its derivative is:

$$n'(\theta) = -\nabla_t(\theta \cdot n) \text{ on } \partial\Omega$$

where $\nabla_t \zeta = \nabla\zeta - (\nabla\zeta \cdot n)n$ is the tangential gradient of a function ζ.

4.1.1 General case

We proceed to the computation of the gradient of a general criterion:

$$J(\Omega) = \int_\Omega m(u)\,dx + \int_{\Gamma_m} l(u)\,ds \tag{26}$$

where Γ_m will be the part of $\partial\Omega$ allowed to move during the optimisation process, m and l are smooth functions verifying

$$|m(u)| \leq C\left(1 + \|u\|^2\right)$$
$$|m'(u)\cdot h| \leq C' \|u\|\,\|h\|$$

and

$$|l(u)| \leq C\left(1 + \|u\|^2\right)$$
$$|l'(u)\cdot h| \leq C' \|u\|\,\|h\|$$

for every $h \in L^2(\Omega)^d$ and $u \in L^2(\Omega)^d$, and with $C > 0$ and $C' > 0$.

In the next theorem, we shall consider the solution u of the nonlinear variational equation (24) which involves the function $j(u,p,n)$ (the precise form of which differs according to the considered penalised and regularised contact model). In order to distinguish the normal derivative $(\partial j)/(\partial n)$ from the partial derivative of $j(u,p,n)$ with respect to its third argument, we now consider j as a function of three arguments $(u,p,\lambda) \in \mathbb{R}^d \times \mathbb{R}^d \times \mathbb{R}^d \to \mathbb{R}$ and the derivative with respect to n of $j(u,p,n)$ is denoted:

$$\frac{\partial j}{\partial \lambda}(u,p,n).$$

Theorem 4.1.2. *Assume that $\Gamma_m \cap \Gamma_0 = \varnothing$, that $f \in H^1(\mathbb{R}^d)^d$ and $g \in H^2(\mathbb{R}^d)^d$, and that $u \in H^1_{\Gamma_0}(\Omega)^d$ is solution of (24) (supposing it exists and is unique). If we denote $J'(\Omega)(\theta)$ the Gâteaux derivative of $J(\Omega)$ with respect to Ω in the direction $\theta \in W^{1,\infty}(\mathbb{R}^d,\mathbb{R}^d)$, we have:*

$$\begin{aligned}
J'(\Omega)(\theta) = &\int_{\Gamma_m} (\theta\cdot n)(m(u) + Ae(u) : e(p) - f\cdot p)\,ds \\
&+ \int_{\Gamma_m} (\theta\cdot n)\left(Hl(u) + \frac{\partial l(u)}{\partial n}\right) \\
&- \int_{\Gamma_N\cap\Gamma_m} (\theta\cdot n)\left(Hp\cdot g + \frac{\partial (p\cdot g)}{\partial n}\right) ds \\
&+ \int_{S\cup\Gamma_c} (\theta\cdot n)\left(Hj(u,p,n) + \frac{\partial j(u,p,n)}{\partial n}\right) ds \\
&+ \int_{S\cup\Gamma_c} \frac{\partial j}{\partial \lambda}(u,p,n)\cdot n'(\theta)\,ds
\end{aligned} \tag{27}$$

where $n'(\theta)$ is the shape derivative of the normal (on S it is the shape derivative of n_-) and p is defined as the solution of the following adjoint problem:

$$\begin{aligned}
&\int_\Omega Ae(p) : e(\psi)\,dx + \int_\Omega m'(u)\cdot\psi\,dx + \int_{\Gamma_m} l'(u)\cdot\psi\,ds \\
&+ \int_{S\cup\Gamma_c} \frac{\partial j}{\partial u}(u,p,n)\cdot\psi\,ds = 0 \quad \forall \psi \in H^1_{\Gamma_0}(\Omega)^d.
\end{aligned} \tag{28}$$

Proof. The proof relies on Céa's method [9] or [1]. A rigorous proof would require to prove that u is Gâteaux differentiable with respect to the shape. This could be done by making in the nonlinear regularised formulation (24) a change of variable to transport integrals on the reference domain Ω_0 such that $\Omega = (Id + t\theta)(\Omega_0)$. This leads to an equation of the type: $F(u,t) = 0$ with F differentiable with respect to t, thanks to Remark 3.3.2 and Lemma 3.3.1. Applying the implicit function theorem at $t = 0$ yields the desired result. Assuming this point proved, we give a (formal) proof of the theorem by means

of the Lagrangian method, noting $u'(\theta)$ the shape derivative of u. Let us introduce the Lagrangian L with v and q in $H^1_{\Gamma_0}(\mathbb{R}^d)^d$:

$$\begin{aligned} L(v,q,n(\Omega),\Omega) &= \int_\Omega m(v)\,dx + \int_{\Gamma_m} l(v)\,ds + \int_\Omega Ae(v):e(q)\,dx \\ &+ \int_{S\cup\Gamma_c} j(v,q,n)\,ds - \int_\Omega f\cdot q\,dx - \int_{\Gamma_N} g\cdot q\,ds. \end{aligned}$$

Recall that $j(v,q,n)$, defined in (24), is a linear function of q. Thus, the Lagrangian L is linear with respect to the adjoint variable q too, as it should be. Since Γ_0 is fixed, there is no need of a Lagrange multiplier for the Dirichlet condition in the Lagrangian: $\Gamma_0 \subset \partial\Omega$ for every $\Omega \in \mathcal{U}_{ad}$. Moreover the functions q and v are in spaces independent of $\Omega \in \mathcal{U}_{ad}$. We note (u,p) a stationarity point of L. The state equation (24) can be retrieved by differentiating L with respect to q in the direction $\psi \in H^1_{\Gamma_0}(\mathbb{R}^d)^d$:

$$\langle \frac{\partial L}{\partial q}(u,q,n,\Omega),\psi\rangle = 0 \quad \forall \psi \in H^1_{\Gamma_0}(\mathbb{R}^d)^d\,.$$

Similarly, the adjoint equation (28), solved by p, is found by differentiating L with respect to v in the direction $\psi \in H^1_{\Gamma_0}(\mathbb{R}^d)^d$:

$$\langle \frac{\partial L}{\partial v}(u,p,n,\Omega),\psi\rangle = \int_\Omega Ae(v):e(\psi)\,dx + \int_\Omega m'(u)\cdot\psi\,dx + \int_{\Gamma_m} l'(u)\cdot\psi\,ds \quad + \int_{S\cup\Gamma_c} \frac{\partial j}{\partial u}(u,p,n)\cdot\psi\,ds$$

and the adjoint variational formulation is deduced by making the above term zero.

To find the shape derivative of $J(\Omega)$, we remark that:

$$J(\Omega) = L(u(\Omega),q,n(\Omega),\Omega)$$

and differentiate L with respect to the shape in the direction θ which gives:

$$\begin{aligned} J'(\Omega,\theta) &= L'(\Omega,u_\Omega,q,n_\Omega;\theta) \\ &= \partial_\Omega L(\Omega,u_\Omega,q,n_\Omega;\theta) + \langle \frac{\partial L}{\partial v}(\Omega,u_\Omega,q,n_\Omega),u'(\theta)\rangle + \langle \frac{\partial L}{\partial \lambda}(\Omega,u_\Omega,q,n_\Omega),n'(\theta)\rangle. \end{aligned}$$

But, as $u'(\theta) \in H^1_{\Gamma_0}(\Omega)^d$, taking $q = p(\Omega)$ leads to:

$$\langle \frac{\partial L}{\partial v}(\Omega,u_\Omega,p(\Omega),n_\Omega),u'(\theta)\rangle = 0.$$

Consequently:

$$J'(\Omega,\theta) = L'(\Omega,u_\Omega,p_\Omega,n_\Omega;\theta) = \partial_\Omega L(\Omega,u_\Omega,p_\Omega,n_\Omega;\theta) + \langle \frac{\partial L}{\partial \lambda}(\Omega,u_\Omega,p_\Omega,n_\Omega),n'(\theta)\rangle.$$

By using the formulae of Theorem 4.1.1, we recover (27). □

Remark 4.1.1. *The derivative found here is correct only if the solution u exists and is unique. Nevertheless, we will use Theorem 4.1.2 even for models where no uniqueness results are known.*

4.2 Criteria

4.2.1 Compliance and volume

In some numerical examples we will use these two classical criteria which can be written under the form of (26). For the compliance:

$$m_{Comp}(u) = f\cdot u$$
$$l_{Comp}(u) = g\cdot u$$

For the volume:

$$m_{vol}(u) = 1$$
$$l_{vol}(u) = 0$$

4.2.2 Normal force

The normal force, which is always non-positive (see (6)), is the force which is applied on the structure at the contact surface. It takes the following form: $Ae(u)n \cdot n$ on Γ_c and $Ae(u|_{S_-})n_- \cdot n_-$ on S. In the penalised and regularised formulations the normal force P_N is now given by a different formula:

$$P_N = \begin{cases} -\frac{1}{\epsilon}\phi_\eta(u \cdot n) & \text{on } \Gamma_c \\ -\frac{1}{\epsilon}\phi_\eta([u] \cdot n_-) & \text{on } S \end{cases} \tag{29}$$

where $\phi_\eta(x)$ was defined in (18) as a smooth approximation of $\max(0, x)$ and ϵ is the penalisation parameter defined in (17).

The various criteria we consider, depending on the normal force, are of the form:

$$l(u) = l_i(P_N(u), c)\mathbb{1}_{S \cup \Gamma_c}$$

where $\mathbb{1}_{S\cup\Gamma_c}$ is the characteristic function of $S \cup \Gamma_c$ and l_i will be defined according to which characteristic of the normal force we want to control.

Uniformisation: If we want to make the force uniform on the contact zone around a constant c, we will use the following function:

$$l_1(P_N, c) = (P_N - c)^2 \tag{30}$$

with $c < 0$.

Minimising the maximum of the normal force: We want P_N to be under a certain threshold $c < 0$. The first natural criterion which arises is of the type:

$$l_2(P_N, c) = \max(P_N - c, 0)^2.$$

However, this could lead to a null gradient during the optimisation process due, for example, to a null adjoint p when there is no point in contact. This could be a big hurdle when the initial shape in the optimisation process is such that there is no contact. Indeed the gradient does not indicate that contact is possible and how to reach a shape where there is an effective contact. So we change the definition of P_N by introducing the following function:

$$\phi_\eta^{th}(x) = \begin{cases} \phi_\eta(x) - \phi_\eta(0) & \text{if } x \geq 0 \\ \phi_\eta'(0)x & \text{otherwise.} \end{cases}$$

We plot the corresponding functions ϕ_η and ϕ_η^{th} on Figure 2. Then we define:

$$P_N^{th} = \begin{cases} -\frac{1}{\epsilon}\phi_\eta^{th}(u \cdot n) & \text{on } \Gamma_c \\ -\frac{1}{\epsilon}\phi_\eta^{th}([u] \cdot n_-) & \text{on } S \end{cases}$$

Now when $u \cdot n = 0$, the normal force is set to 0 and when $u \cdot n < 0$, the force is nonnegative and decreases linearly, giving a sense to an opposite normal force when there is no contact. Making the most of this new normal force formulation, we define the following criterion:

$$l_3(P_N^{th}, c) = \begin{cases} 1 - \frac{P_N^{th}}{c} & \text{if } P_N^{th} \leq 0 \\ e^{-\frac{P_N^{th}}{c}} & \text{if } P_N^{th} > 0. \end{cases} \tag{31}$$

The bigger $\frac{P_N^{th}}{c}$, the smaller is $l_3(P_N^{th}, c)$. Other formulas for l_3 are also possible and give results similar to those obtained with (31).

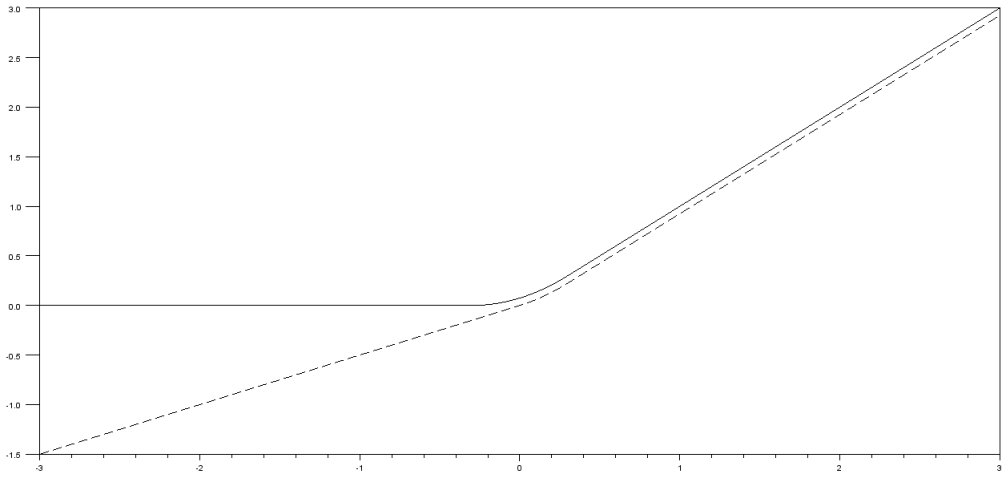

Figure 2: The functions ϕ_η (continuous curve) and ϕ_η^{th} (dashed curve).

5 Numerical implementation

5.1 The level set method

As we choose to define the shape thanks to a level set, we recall the framework of this method introduced by Osher and Sethian in [45], [44] and [52]. Let $D \subset \mathbb{R}^d$ be a bounded domain in which all admissible shapes Ω are included. The boundary of Ω is located thanks to the level set function ψ, defined in D by

$$\begin{cases} \psi(x) = 0 & \text{if } x \in \partial\Omega \cap D \\ \psi(x) < 0 & \text{if } x \in \Omega \\ \psi(x) > 0 & \text{otherwise} \end{cases}$$

The normal n and the mean curvature H of the shape Ω are respectively given by $\dfrac{\nabla\psi}{\|\psi\|}$ and $\operatorname{div}\left(\dfrac{\nabla\psi}{\|\psi\|}\right)$. These quantities are computed throughout the whole domain D which naturally defines extensions of their first definition on $\partial\Omega$.

5.2 Optimisation algorithm

The optimisation process produces a sequence $(\Omega_i)_{i\in\mathbb{N}}$ of shapes. We start with an initial shape Ω_0 and compute iteratively the sequence. To make the level set evolve from Ω_i to Ω_{i+1}, the Hamilton Jacobi transport equation [45] is solved for $t \in [0, t_f]$:

$$\frac{\partial\psi}{\partial t} + V\|\nabla\psi\| = 0 \text{ in } D \tag{32}$$

where $V(x)$ is the normal velocity of the shape's boundary. The equation (32) is obtained by differentiating: $\psi(t, x(t)) = \text{Cst}$ and replacing $\dot{x}(t)$ by Vn. Thanks to $\psi(x,t)$ we can define $\Omega_i(t)$ for every $t \in [0, t_f]$ and choose $\Omega_{i+1} = \Omega_i(t_f)$ for an appropriate t_f which corresponds to the descent step. The speed V, defined everywhere in D to be able to solve (32), is chosen, through a SLP type algorithm, thanks to the criteria's gradients calculated on Ω_i using theorem 4.1.2 and plays the role of a descent direction.

The Hamilton-Jacobi equation (32) is solved by an explicit second order upwind scheme on a cartesian grid meshing D with Neumann boundary conditions. Since the scheme is explicit in time, the time stepping has to satisfy a CFL condition and, in order to regularise the level set which can become too flat or too steep during the successive optimisation iterations, periodic reinitialisations, thanks to an Hamilton Jacobi equation admitting the signed distance to the shape as stationnary solution, are performed. We refer to [2] for numerical implementation details.

5.3 Finite element method

Using the same cartesian grid, we choose to solve the contact and adjoint equations on the whole domain D using the "ersatz material" approach, thanks to the quadrangular finite elements. It is tantamount to fill $D \setminus \Omega$ with a weak material mimicking void but preventing the stiffness matrix from being singular. This technique is commonly used in topology optimisation with level sets [2], [60].

Concerning the nonlinear penalised equations, they are usually solved by a damped Newton method, see [11] chapter 6, or a fixed point method. The Newton method has the advantage to be faster but it needs a good choice for the damping. On the other hand, the fixed point method despite its relative slowness is easier to implement. The robustness of the algorithm which solves the contact equations is crucial in the optimisation process. First because the optimisation can produce structures for which the finite element matrices are nearly singular. Secondly because we are solving problems whose solution is not always unique. This leads to difficulties which can be seen in examples 11 and 12 below. The contact problems are solved (thanks to the finite element method) by discretising the contact region and applying node to node contact conditions for the auto-contact part. We choose to use a fixed point method for the computation of the nonlinear problems solutions considered, which converges in, at most, 300 iterations with an average of 100.

6 Numerical examples

This section is divided into two subsections corresponding respectively to 2D and 3D examples. In all the examples of this section, the contact zone is fixed (non-optimisable) but the structure can choose to use it or not. In each subsection, different models are used depending on the mechanical case. In 2D, except for examples 5, 11 and 12, the domain D is a square of size 2×2 discretised with 6400 square elements. For the other examples, D is a square of size 2×2 discretised with 2500 square elements. For the 3D examples, only the sliding contact problem and Tresca friction contact problem are tested. Except in example 14 where D is a cylinder of radius 1 and of height equal to 1, the domain D is a rectangular parallelepiped of dimension $1 \times 2 \times 1$ meshed with tetrahedra. In every 2D example, the Young modulus is set to $E = 1$ and Poisson ratio to $\nu = 0.3$, there is no volume force and only unit surface forces are applied (point loads for all cases, except for example 3 where it is a constant line load). In 3D examples, we take $E = 210000$ and $\nu = 0.3$. In 2D and 3D, the penalisation coefficient ϵ is set to 10^{-7}. During the optimisation process, some shapes are rejected either because they do not fullfill the constraints or because they do not decrease the objective function. Due to this fact, for each example, both the number of iterations (shapes which were accepted) and the number of evaluations (all the shapes which were evaluated) are given.

6.1 Examples in 2D

6.1.1 Sliding contact

We present five examples (labeled from 1 to 5) where the volume is minimised under a compliance constraint (the value of this constraint is given in Table 1). The potential contact zone is drawn in green, the arrows represent the forces and black zones the part of the boundary where Dirichlet conditions are prescribed, in all the directions (otherwise mentioned). The results are collected in Table 1.

- Example 1, Dirichlet conditions are enforced on the whole left side and a downward unit force is applied at the point $(2, 1.5)$. Results are shown in Figure 3.
- Example 2, Dirichlet conditions are enforced on the whole left side and a unit downward force is applied at the point $(2, 1.5)$. Example 1-2bis is the same example as 1 and 2 without the contact zone. Results are presented in Figures 4 and 5.
- Example 3, Dirichlet conditions are enforced on the whole left side and a rightward unit constant force is applied on the segment from $(2, 0.8)$ to $(2, 1.2)$. Example 3bis is similar without the contact area. Results are given in Figures 6 and 7.

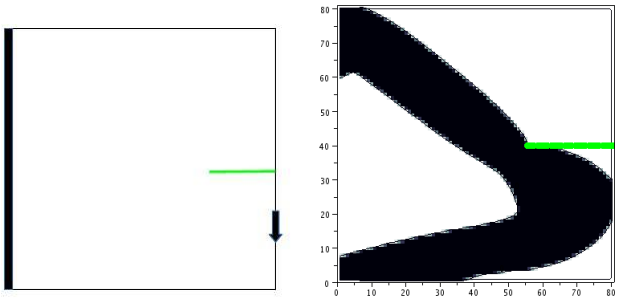

(a) Load case for Example 1 (b) Final design for Example 1

Figure 3: Example 1

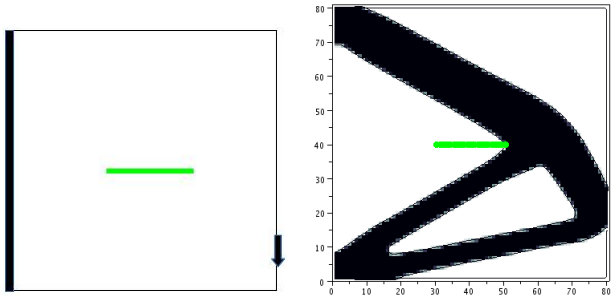

(a) Load case for Example 2 (b) Final design for Example 2

Figure 4: Example 2

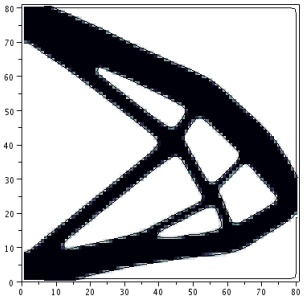

Figure 5: Final design for Example 1-2bis

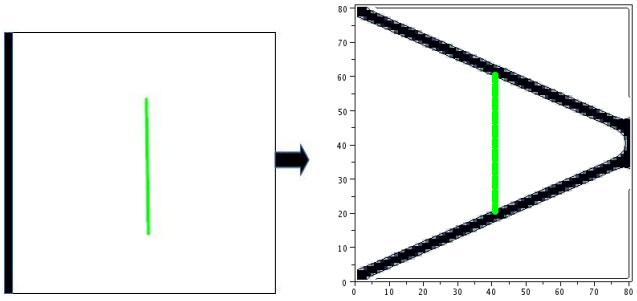

(a) Load case for Example 3 (b) Final design for Example 3

Figure 6: Example 3

- Example 4, Dirichlet conditions are enforced on the whole left side and a unit upward force is

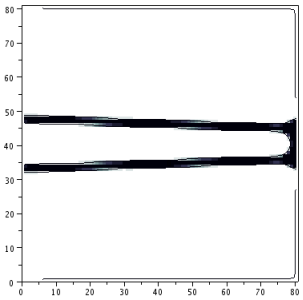

Figure 7: Final design for Example 3bis

applied at $(2, 1.5)$. Example 4bis is similar without the contact boundary conditions. Results can be seen in Figures 8 and 9.

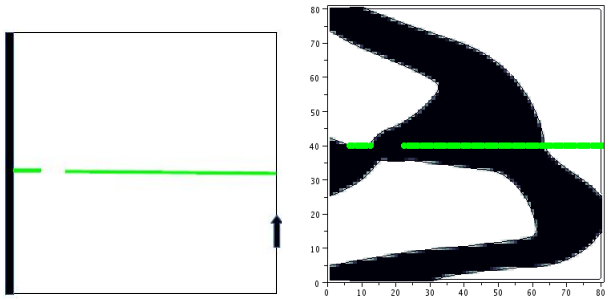

(a) Load case for Example 4 (b) Final design for Example 4

Figure 8: Example 4

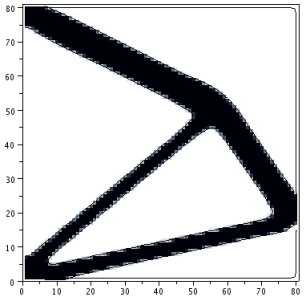

Figure 9: Final design for Example 4bis

- Example 5, Dirichlet conditions are enforced on the top boundary of the L-shape and a unit downward force is applied at $(2, 1.6)$. Example 5bis corresponds to the same problem without the contact part. Results are shown in Figures 10 and 11.

In examples 1, 2, and 3, the optimisation algorithm tends to avoid the contact zone which is not the case when this zone is removed. Indeed, due to the direction of the forces, this zone opens and no point is in contact. Including it in the structure would increase the compliance, which is not possible by virtue of the constraint on the compliance. In example 4, the points of the contact zone are in contact and including them in the structure does not imply a too big increase of the compliance, despite the sliding occuring. In example 5, the contribution of the contact boundary conditions is underlined by the fact that, for the same optimisation problem without contact (example 5bis), even the full-domain solution is not admissible (its compliance is about 118). We need to weaken the compliance constraint to have a feasible starting solution for the optimisation algorithm in the case of example 5bis.

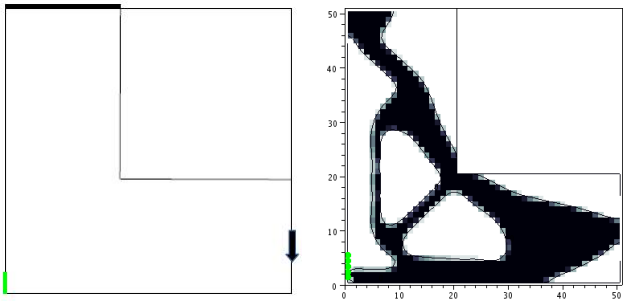

(a) Load case for Example 5 (b) Final design for Example 5

Figure 10: Example 5

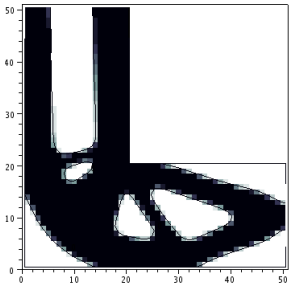

Figure 11: Final design for Example 5bis

In the next four examples (labeled from 6 to 9), the normal force criteria (30) and (31) are used to obtain different kinds of clamps or gripping mechanisms. Apart from example 6, in which the normal force criterion is minimised under volume and compliance constraints, we minimise the volume under compliance and normal force constraints (the precise values of these constraints are given in Table 2 and 3). The results are presented in Tables 2 and 3.

- Example 6, here the Dirichlet conditions at $(1.9, 0)$ and $(1.9, 2)$ are put only for the x (horizontal) part of the displacement and two unit forces are applied at $(1.8, 2)$ and $(1.8, 0)$. The normal force criterion used is l_3 with $c = -1.5$. See Figure 12 for the results.

  The shape of a clamp is found, which manages to bring the forces from the right side to the left side, keeping their direction. We remark that we do not manage to reach the value of the threshold c. In the next example, we will use the same criterion as a constraint and see that the results are far better on this particular point.

- Example 7, two unit forces are applied at $(1.8, 2)$ and $(1.8, 0)$ and the structure is fixed from $(2, 0.9)$

Cases	Volume	Compliance	Compliance Constraint	Iterations	Evaluations
1	1.6403	19.9999	20	66	92
2	1.45211	19.9998	20	67	95
1-2bis	1.41650	19.9997	20	22	38
3	0.35078	0.499995	0.5	82	110
3bis	0.248584	0.499993	0.5	31	47
4	1.69044	29.9999	30	64	95
4bis	0.928932	29.9841	30	28	46
5	1.15278	94.9829	95	18	36
5bis	1.64209	139.906	140	18	35

Table 1: Results for sliding contact examples and examples 1-2bis, 3bis, 4bis and 5bis.

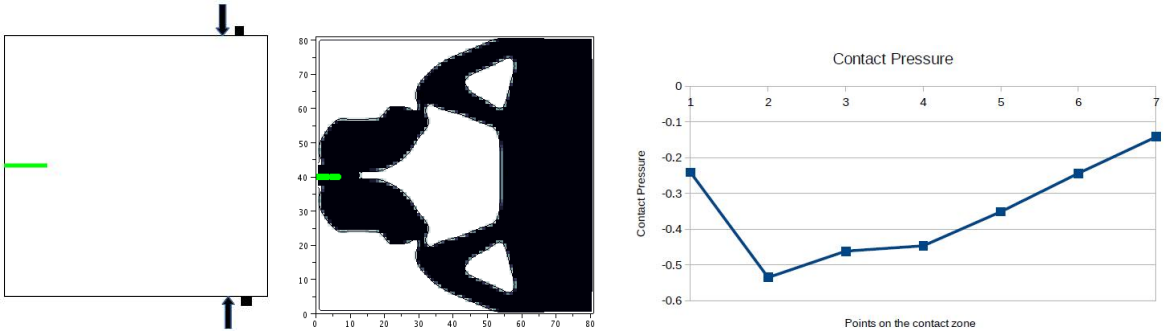

(a) Load case for Example 6 (b) Final design for Example 6 (c) Final normal force (in blue) for Example 6

Figure 12: Example 6

to $(2, 1.1)$. The normal force criterion used is l_3 with $c = -1.1$. We refer to Figure 13 for the results.

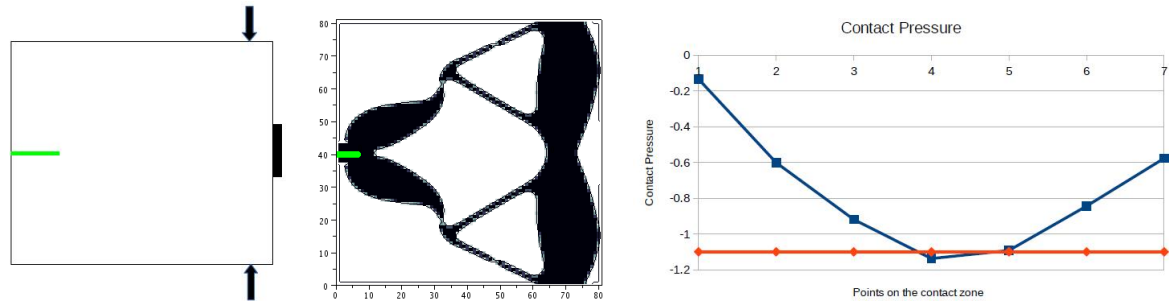

(a) Load case for Example 7 (b) Final design for Example 7 (c) Final normal force (in blue) and the threshold c (in red) for Example 6bis

Figure 13: Example 7

The Dirichlet part on the right side is used at the beginning of the optimisation process and is finally found to be useless.

- Example 8, two unit forces are applied at $(1.5, 2)$ and $(1.5, 0)$. Dirichlet conditions are enforced on the whole left side. The normal force criterion used is l_3 with $c = -0.9$. Figure 14 presents the results.

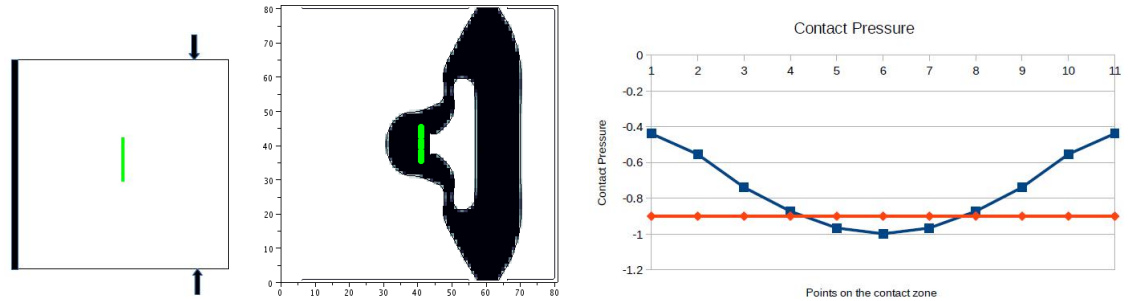

(a) Load case for Example 8 (b) Final design for Example 8 (c) Final normal force (in blue) and the threshold c (in red) for Example 8

Figure 14: Example 8

On the contrary, this example shows a mechanism which transforms the vertical forces into horizontal ones.

Cases	Norm. force	Compl.	Compl. Constr.	Vol.	Vol. constr.	Iterations	Evaluations
6	3.03302	8.32621	8.4	2.27271	2.7	16	23

Table 2: Results for the Example 6.

Cases	Vol.	Compl.	Compl. Constr.	Norm. force	Norm. force Constr.	Iterations	Evaluations
7	1.34868	10.9603	11	1.99976	2	251	275
8	0.971308	5.99801	6	1.49998	1.5	178	206
9	1.62217	14.9941	15	0.148007	0.15	24	40

Table 3: Results for Examples 7, 8 and 9

- Example 9, the downside is fixed and two unit forces are applied at $(0.2, 0)$ and $(1.8, 0)$. The normal force criterion used is l_1 with $c = -2$. Figure 15 gives the results.

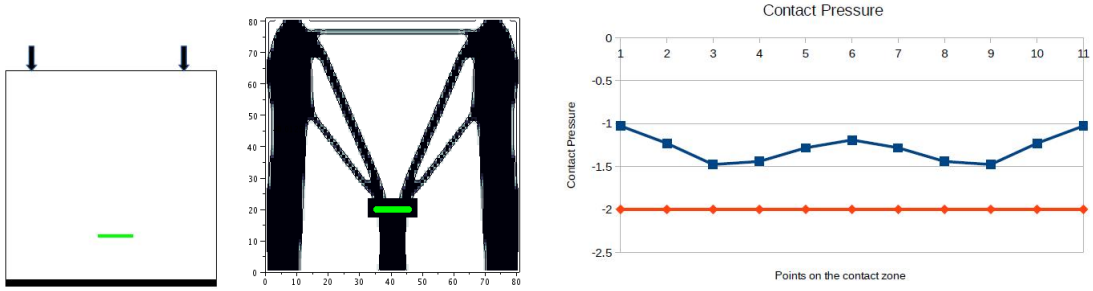

(a) Load case for Example 9

(b) Final design for Example 9

(c) Final normal force (in blue) and the threshold c (in red) for Example 8

Figure 15: Example 9

Finally Example 9 produces pilars that are not perpendicular to the Dirichlet zone to put weight on the contact zone.

For theses examples (6 to 9), it has to be noted that the computation of the normal force, thanks to the penalisation formula (29), is not very accurate since the displacement u is multiplied by the large penalisation factor $1/\epsilon$. Therefore, if one requires a precision of the order of unity for the normal force, the displacement u should be solved with a precision smaller than ϵ, which is not the case here. Moreover, it appears that the criteria used are quite sensitive to small changes in the shape. This forbids the use of too tight normal force constraints, which explains that pointwise constraints are most of the time not exactly fullfilled. These examples are however interesting as they give a good hint of the possible optimal shape for pointwise constraints.

6.1.2 Contact with friction

We give four examples (labeled from 10 to 13) of contact optimisation with friction. For each of these examples, the results are displayed for all contact models: sliding (no friction), Tresca, Norton Hoff, normal compliance and Coulomb. The friction coefficient is σ_{tr} for the Tresca model and μ for all other models. For the normal compliance model, we have $C_N = 1$, $m_N = 1$ and $m_T = 1$. For the Norton Hoff model, we recall that ρ denotes the exponent parameter defined in (13). We minimise the volume under a compliance constraint.

- Example 10, a unit force is applied at $(2, 1)$, the left side of the structure is fixed. The friction coefficient is 0.5 and for the Norton Hoff model $\rho = 0.1$. Example 10bis corresponds to the same problem without the two contact areas. Results can be found in Table 4 and Figures 16 and 17.

  In all the cases, the algorithm tends to avoid the upper contact zone which opens and keep the lower one. However, in sliding contact, the lower leg has to be hooked up to a part of the structure

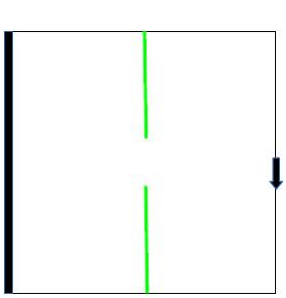

(a) Load case for Example 10

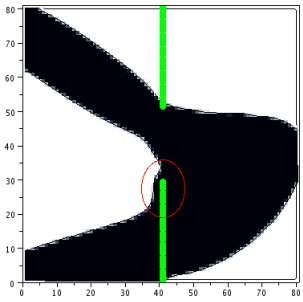

(b) Final design for frictionless contact

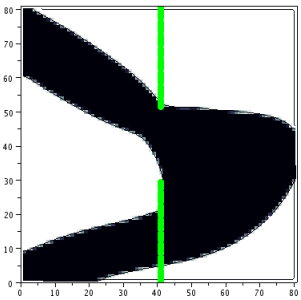

(c) Final design for the Tresca model

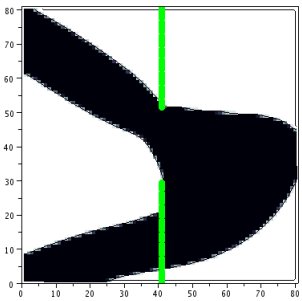

(d) Final design for the Norton-Hoff model

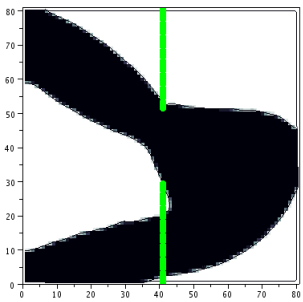

(e) Final design for the normal compliance model

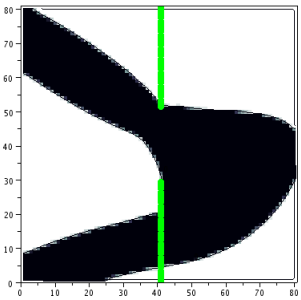

(f) Final design for the Coulomb model

Figure 16: Example 10

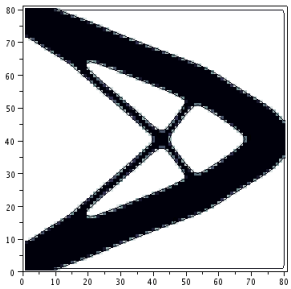

Figure 17: Final design for Example 10bis (without contact).

which is not in the contact zone. It is not the case in the friction cases as the friction keeps the lower leg connected to the structure (see the zone circled in red on the final design for frictionless contact and the equivalent zone on the models with friction). The Example 9bis is meant to underline the impact of the contact on the optimised structure.

Cases	Volume	Compliance	Compliance Constraint	Iterations	Evaluations
Sliding contact	1.87253	19.9998	20	47	73
Tresca	1.76836	19.9999	20	47	73
Norton Hoff	1.76906	19.9999	20	41	67
Normal compliance	1.97197	19.9999	20	49	65
Coulomb	1.76948	19.9998	20	45	70
10bis	1.34787	19.9978	20	33	50

Table 4: Comparison results of friction models for Examples 10 and 10bis.

- Example 11, a unit force is applied at $(1, 2)$. The friction coefficient is 1.3 and for the Norton Hoff model $\rho = 0.5$. The results are delivered in Table 5 and in Figure 18.

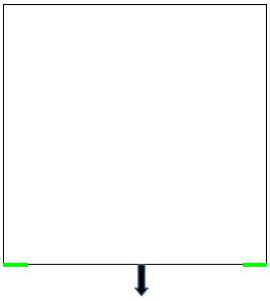

(a) Load case for Example 11

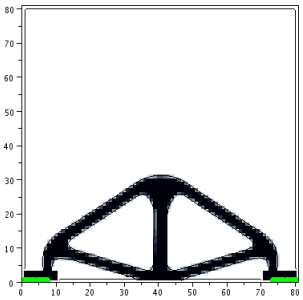

(b) Final design for frictionless contact

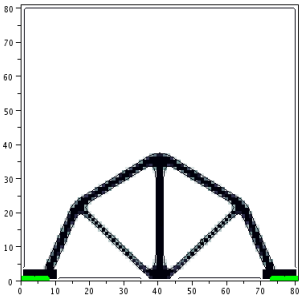

(c) Final design for the Tresca model

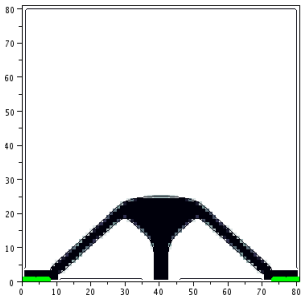

(d) Final design for the Norton-Hoff model

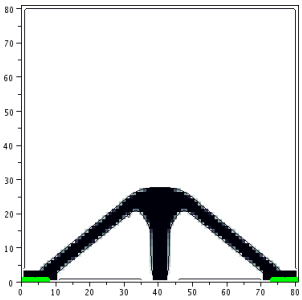

(e) Final design for the normal compliance model

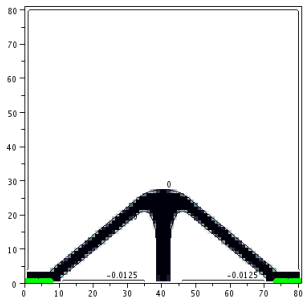

(f) Final design for the Coulomb model

Figure 18: Example 11

In sliding contact the legs of the bridge have to be vertical to the contact zone to prevent sliding. Whereas in other cases, the friction stabilises the structure and enables the legs to incline.

- Example 12, Dirichlet conditions are enforced on the left up part of the L-shape and a downward

Cases	Volume	Compliance	Compliance Constraint	Iterations	Evaluations
Sliding contact	0.422235	21.9991	22	44	71
Tresca	0.302352	21.9957	22	45	71
Norton Hoff	0.309498	21.9995	22	44	65
Normal compliance	0.336178	21.9996	22	37	63
Coulomb	0.286532	21.9995	22	35	61

Table 5: Comparison results of friction models for Example 11.

unit force is applied at $(2, 1.6)$. The friction coefficient is 1.2 and for the Norton Hoff model $\rho = 0.6$. Results are given in Table 6 and Figure 19.

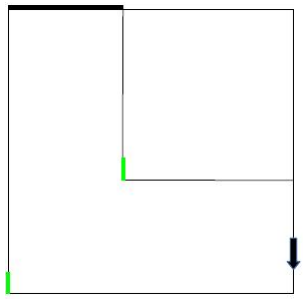

(a) Load case for Example 12

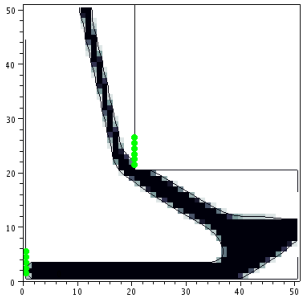

(b) Final design for frictionless contact

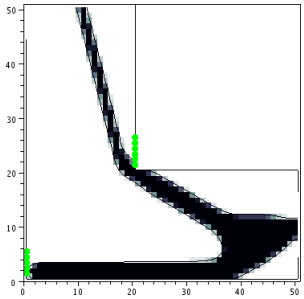

(c) Final design for the Tresca model

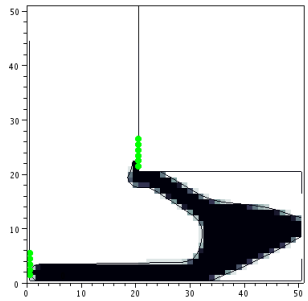

(d) Final design for the Norton-Hoff model

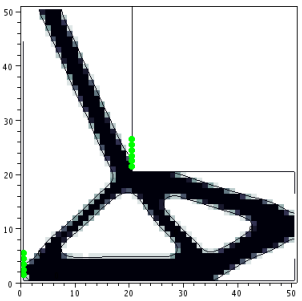

(e) Final design for the normal compliance model

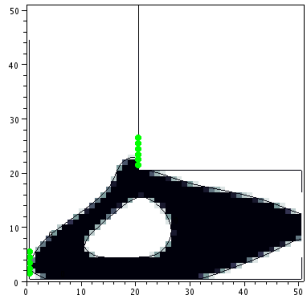

(f) Final design for the Coulomb model

Figure 19: Example 12

The result in sliding contact can be compared with example 5. Here the algorithm makes use of the second contact zone and, for the Norton-Hoff model, manages to use it to stabilise the structure without being connected to the Dirichlet boundary. In the case of Coulomb model, there is trouble in solving the contact problem (for several shapes, the nonlinear algorithm does not converge and

Cases	Volume	Compliance	Compliance Constraint	Iterations	Evaluations
Sliding contact	0.593907	94.9994	95	22	40
Tresca	0.59725	94.9014	95	18	34
Norton Hoff	0.550918	94.5404	95	18	34
Normal compliance	0.917105	94.1346	95	13	30
Coulomb	0.907396	94.9978	95	48	67

Table 6: Comparison results of friction models for Example 12.

the displacement used for computing the shape gradients and the criteria are not accurate enough) which leads to a bad optimised result in terms of volume compared to the other models.

- Example 13, Dirichlet conditions are enforced from $(1.2, 0)$ to $(2, 0)$ and a downward unit force is applied at $(2, 1.6)$. The friction coefficient is 0.8 and, for the Norton Hoff model, $\rho = 0.6$. For example 13bis, we only remove the contact zone. Results are shown in Table 7 and Figures 20 and 21.

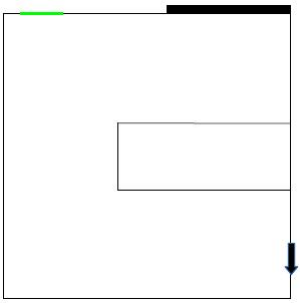

(a) Load case for Example 13

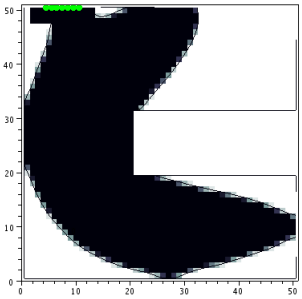

(b) Final design for frictionless contact

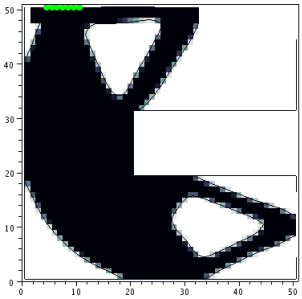

(c) Final design for the Tresca model

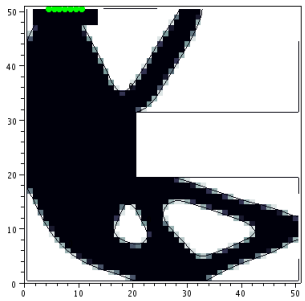

(d) Final design for the Norton-Hoff model

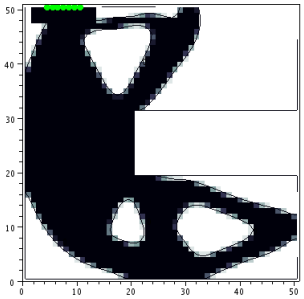

(e) Final design for the normal compliance model

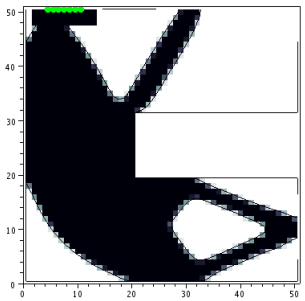

(f) Final design for the Coulomb model

Figure 20: Example 13

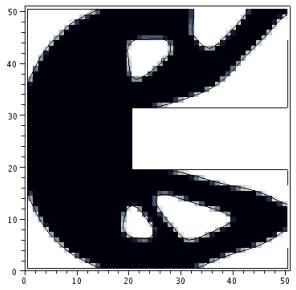

Figure 21: Final design for Example 13bis

Cases	Volume	Compliance	Compliance Constraint	Iterations	Evaluations
Sliding contact	2.15435	149.999	150	16	32
Tresca	1.95836	149.989	150	14	29
Norton Hoff	1.87089	149.881	150	25	40
Normal compliance	1.94898	149.994	150	13	28
Coulomb	1.83706	149.997	150	20	39
13bis	2.39942	149.962	150	20	36

Table 7: Comparison results of friction models for Examples 13 and 13bis.

The contact area enables the structure to be only connected with the Dirichlet part by its left edge and to use less material. The friction allows to slightly decrease the volume.

6.2 Examples in 3D

The following examples (labeled from 14 to 18) were computed thanks to the finite element software SYSTUS of ESI-Group [16]. The nonlinear problems are solved thanks to a Newton algorithm. In all cases, the volume is minimised under a compliance constraint. The friction coefficient is set to 0.01. In examples 15 to 18 we impose a small non-optimisable zone, filled with material, near the boundaries where the Dirichlet condition and and the surface force are applied. In example 14 this is done only for the force zone. To be sure that the models of sliding contact and Tresca were the same as in 2D, we choose to use node to node elements (string elements) for which we implement the penalisations adapted to the frictionless contact and the Tresca model.

- Example 14, for 97289 elements and 17290 nodes. A constant downward surface force equal to 10000 is applied on a square of side 0.2 in the middle of the right face. Dirichlet conditions are enforced on the left face (see Figure 22). The results are gathered in Table 8 and in Figures 22, 23 and 24.

  This example is the equivalent of 2D example 10, but in 3D. The same remark as in frictionless contact applies: the lower leg needs to be hooked up to a part of the structure not containing the contact. This is not the case when friction is possible.

- Example 15, for 156417 elements and 27312 nodes. See Table 9 and Figures 25, 26 and 27 for the results.

  Here there are three circular potential contact zones and the forces are applied on two small cylinders in the middle. Two constant downward surface forces of magnitude 200000 are applied

Cases	Volume	Compliance	Compliance Constraint	Iterations	Evaluations
Sliding contact	2.521889e-01	9.994017e+03	10000	15	23
Tresca	2.555368e-01	9.999298e+03	10000	17	25

Table 8: Comparison results of friction models for Example 14.

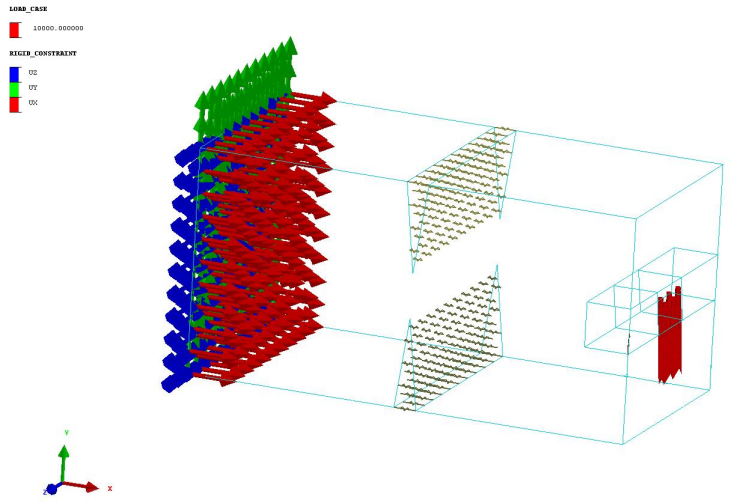

Figure 22: Load case for Example 14.

Cases	Volume	Compliance	Compliance Constraint	Iterations	Evaluations
Sliding contact	2.078838e-01	9.987082e+03	10000	29	40
Tresca	1.920865e-01	9.987843e+03	10000	36	45

Table 9: Comparison results of friction models for Example 15.

on a disk of 0.1 radius at the center of each circular face. Dirichlet conditions are enforced on the bottom face on a ring of thickness 0.1 surrounding the structure (see Figure 25). In both cases the contact zones are enough to stabilise the structure and the Dirichlet zone is not used. Between frictionless and friction contact, slight changes appear in the shape of the three feet of the structure.

- Example 16, for 89475 elements and 15895 nodes. Table 10 and Figures 28 and 29 show the results.

  The cylinder in the center and the bottom left side are completely fixed. A constant downward force of magnitude 50000 is applied on a rectangular part of the bottom face of dimension 0.1×1 on the far right (see Figure 28). As the cylinder in the center is fixed, the algorithm uses it to stabilise the structure. In the frictionless case it needs to turn around the cylinder as sliding is possible. In the friction case this is not needed anymore, but we remark that a small part of material remains under the cylinder, going to it from the base. This part is not in contact but the tangential displacements are such that friction occurs (which is one of the problems of the Tresca model making it non mechanically correct).

- Example 17, for 89475 elements and 15895 nodes. Table 11 and Figures 30, 31 and 32 gather the results.

  A constant downward force of magnitude 50000 is applied on the whole cylinder axis and on the left and right bottom parts, a rectangular part of dimension 0.1×1 is fixed. The cylinder is encircled by material to be supported (see Figure 30). The differences between the sliding and the friction case come from the fact that in the friction case the optimisation algorithm stopped prematurely due to convergence problems in the contact solver.

Cases	Volume	Compliance	Compliance Constraint	Iterations	Evaluations
Sliding contact	7.082515e-01	9.990895e+03	10000	14	23
Tresca	6.915364e-01	9.979266e+03	10000	14	22

Table 10: Comparison results of friction models for Example 16.

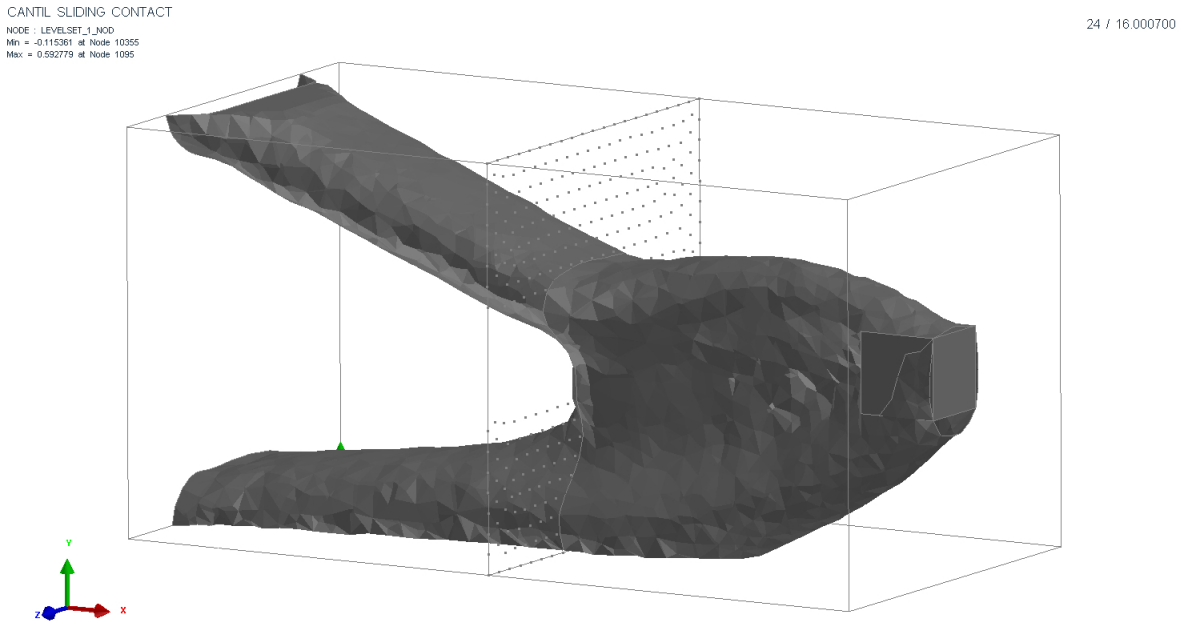

(a) Final design for frictionless contact

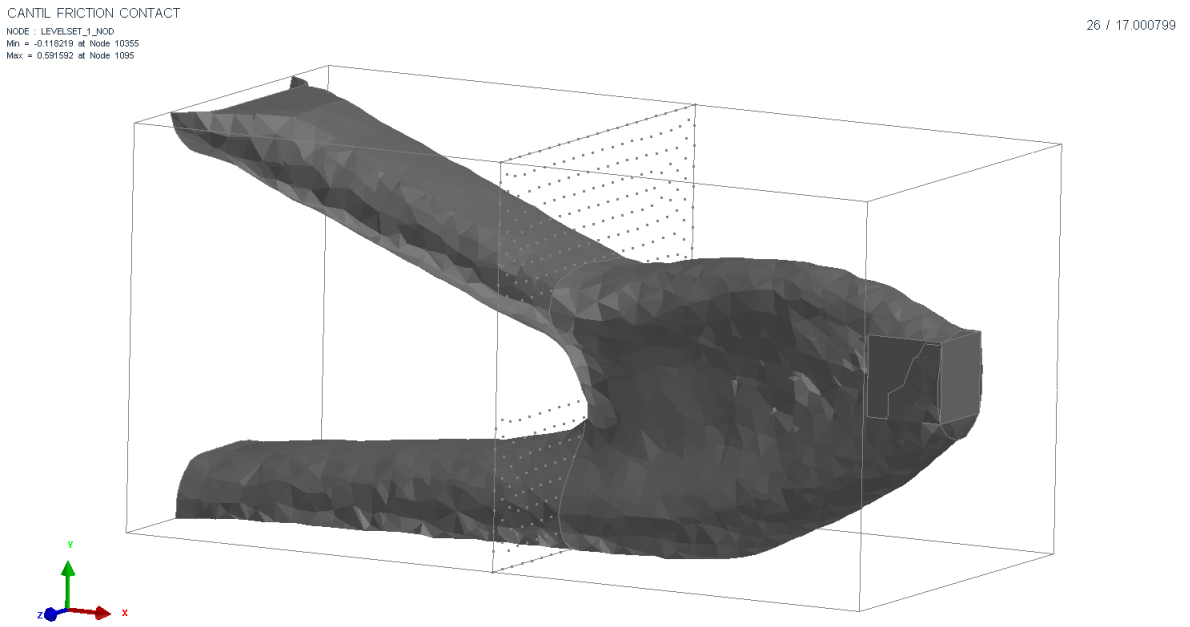

(b) Final design for the Tresca model

Figure 23: Example 14

- Example 18, for 90205 elements and 16010 nodes.Table 12 and Figures 33 and 34 present the results.

  The cylinder is fixed only in the y and x directions. A constant downward force of magnitude 20000 is applied on the whole cylinder axis and two constant downward forces of magnitude 50000 are applied on two rectangular parts of the downside face of dimension 0.1×1 on the far right and the far left. Finally we fix two parts on the bottom. The structure only needs to support the

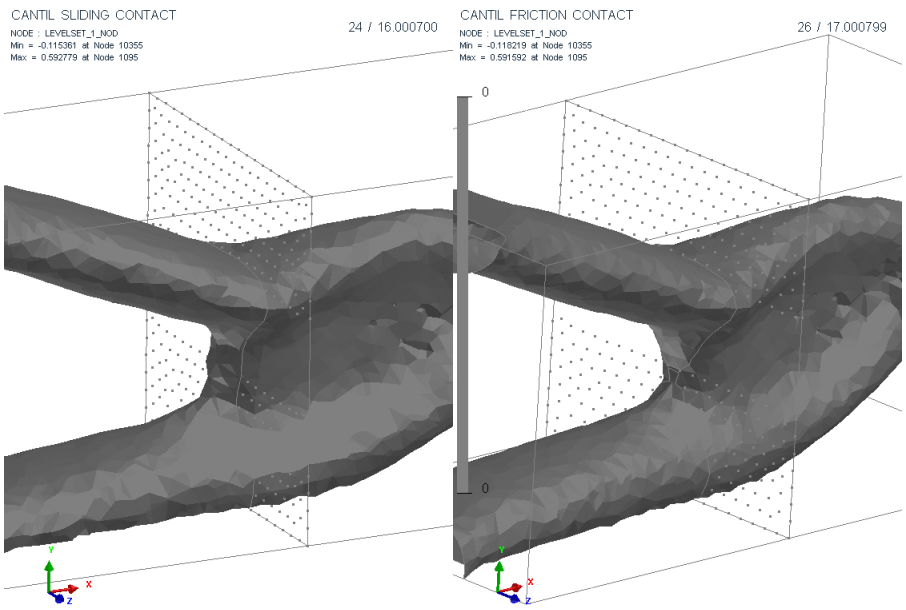

Figure 24: Comparison between without (left) and with (right) friction. We remark the small amount of matter needed only in the sliding case.

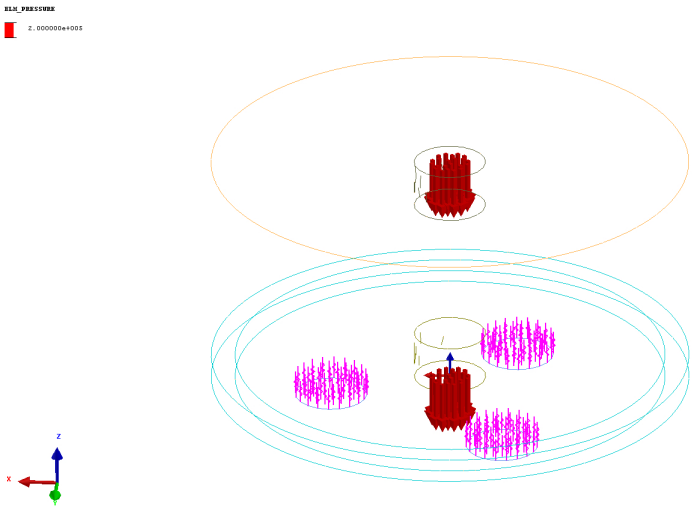

Figure 25: Load case for Example 15.

cylinder and the forces on the left and right side (see Figure 33 for details). To perform that, it uses archways in order to lead to the middle of the structure forces on the sides, changing their direction in the opposite one and, this way, using them to support the force of the cylinder. Due to the Dirichlet conditions put on the cylinder, the fact that the results are the same with or without friction is not a surprise.

7 Conclusion

Through all the numerical examples shown in this article, the regularised and penalised formulations are proved to be good ways to cope with the non differentiability of problems having a unique solution. Despite the possible non uniqueness of its solution, the Norton Hoff model behaves well in this framework.

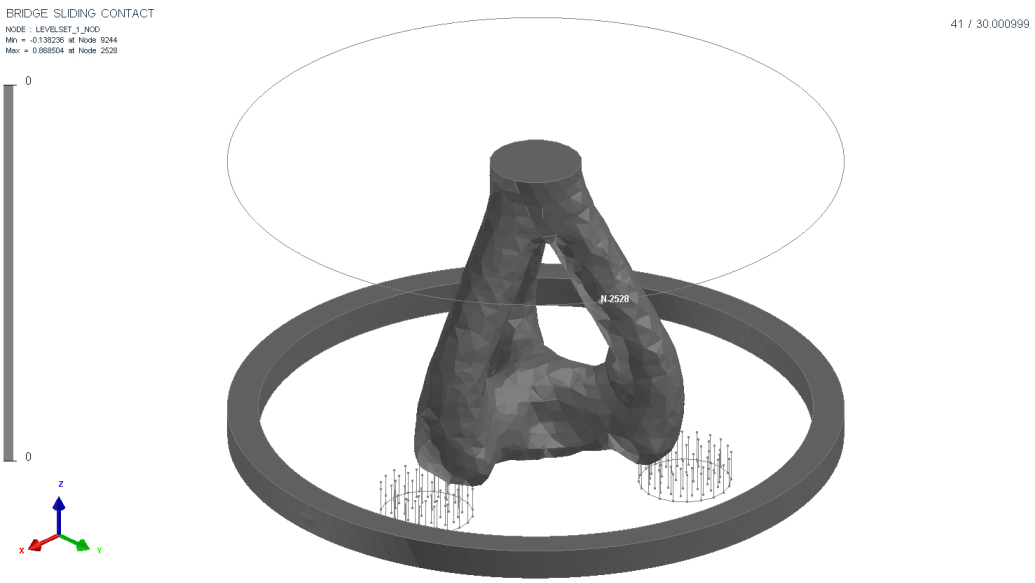

(a) Final design for frictionless contact

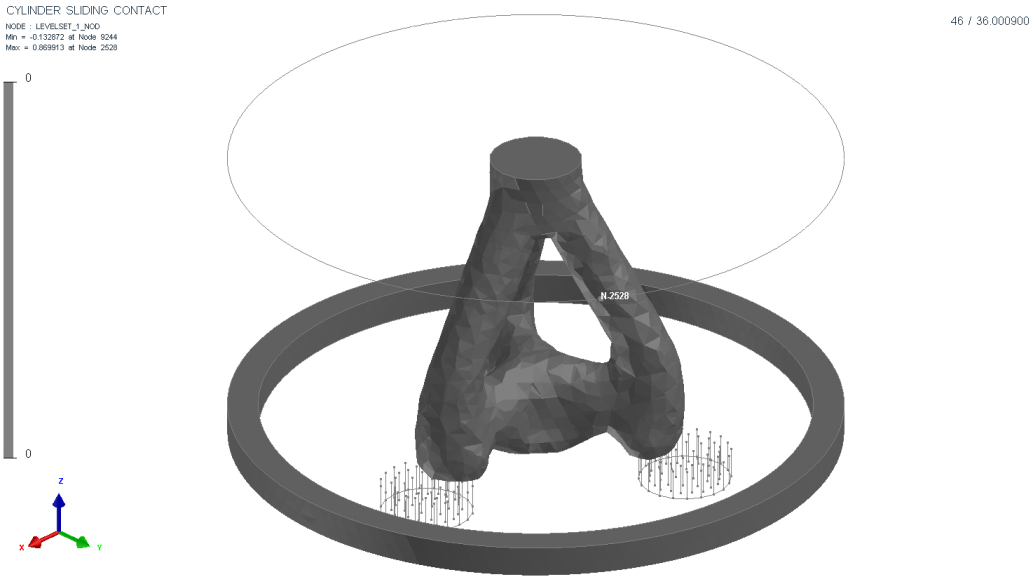

(b) Final design for the Tresca model

Figure 26: Example 15

On the contrary, the Coulomb model presents some difficulties due to a bad convergence in the contact solver. It then appears that the crucial point is the robustness of the contact solver which has to converge in every situation for the optimisation process to succeed. In 3D we used a Newton method to solve the contact problem. It is a good practice (compared to a fixed point algorithm) since it furnishes the tangent matrix M which is precisely the transpose of the stiffness matrix for the adjoint problem. This was of great help for our implementation in the ESI group software.

Concerning the criteria depending on the normal force, we have to be cautious with our numerical results, as the approximations made (Finite element method with penalisation) may not allow a sufficiently correct accuracy on the computed force. However, these criteria can be used to create compliant mechanisms such as in Examples 6, 6bis and 7 or in [39], or, as in Example 8, to get a shape which tends to uniformise the normal force.

To go one step beyond our approach, we could eliminate the regularisation and work in the context

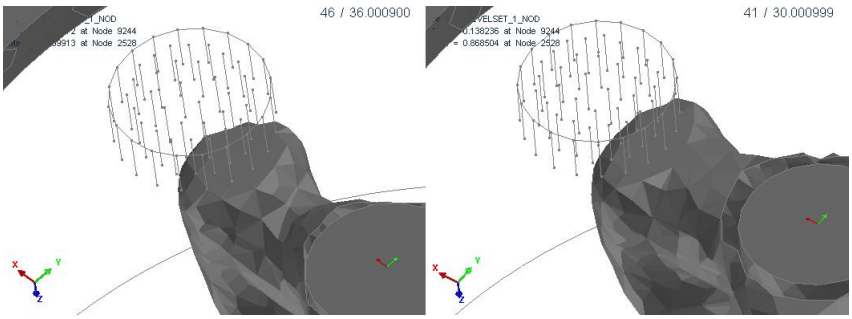

Figure 27: Comparison between with (left) and without (right) friction. We remark that the shape of the foot is larger when friction is present.

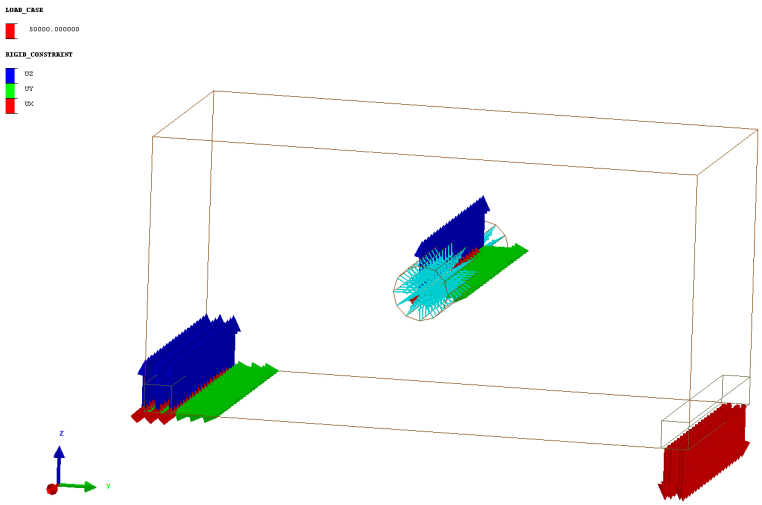

Figure 28: Load case for Example 16.

of non-smooth optimisation. In such a case, one has to use subgradients algorithms. Subgradients were computed for the problems written as variational inequalities in [30] and [47]. It yields a better accuracy on the normal force and gives good results for optimisation with Coulomb friction [6]. Note that [6], [30] and [47], focus on the optimisation of the discrete problem. Finally contact time-dependent problems could also be studied.

Acknowledgements This work has been supported by the RODIN project (FUI AAP 13). The second author G.Allaire is a member of the DEFI project at INRIA Saclay Ile-de-France.The authors acknowledge the help of Philippe Conraux and Damien Lachouette (ESI group) for the computations performed with the SYSTUS code.

Cases	Volume	Compliance	Compliance Constraint	Iterations	Evaluations
Sliding contact	3.293794e-01	9.997417e+03	10000	78	87
Tresca	3.322390e-01	9.860692e+03	10000	22	33

Table 11: Comparison results of friction models for Example 17.

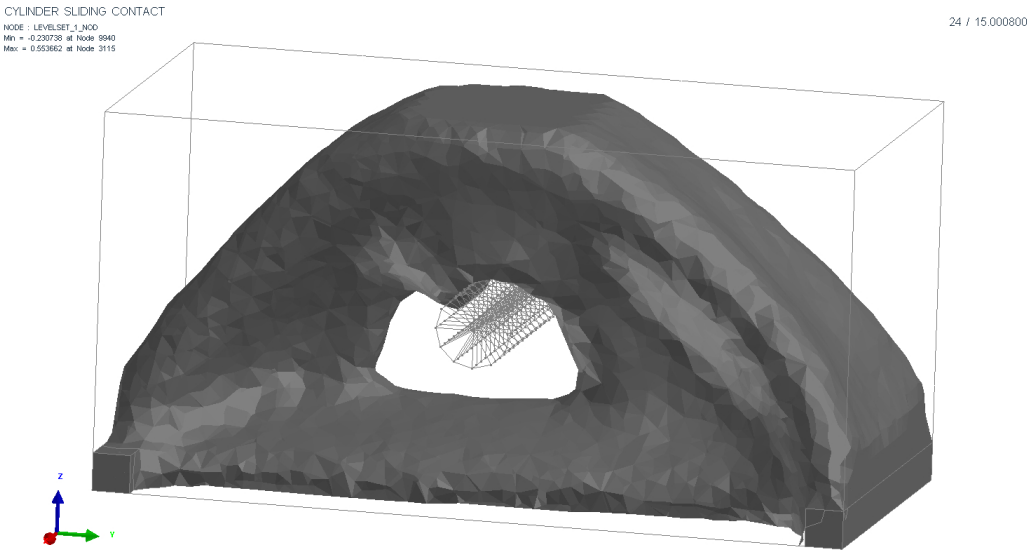

(a) Final design for frictionless contact

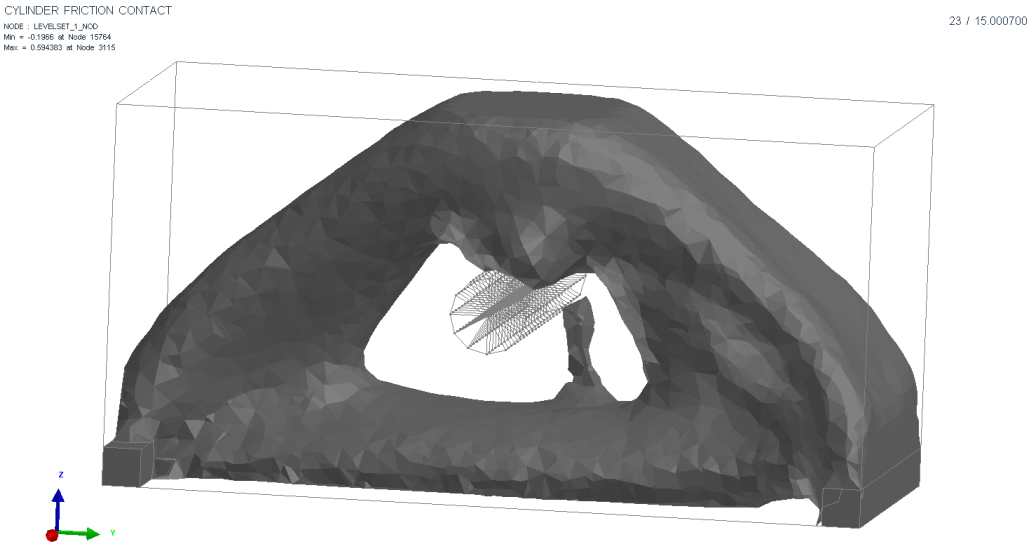

(b) Final design for the Tresca model

Figure 29: Example 16

Cases	Volume	Compliance	Compliance Constraint	Iterations	Evaluations
Sliding contact	2.349350e-01	1.981722e+04	20000	81	89
Tresca	2.299134e-01	1.986286e+04	10000	100	111

Table 12: Comparison results of friction models for Example 18.

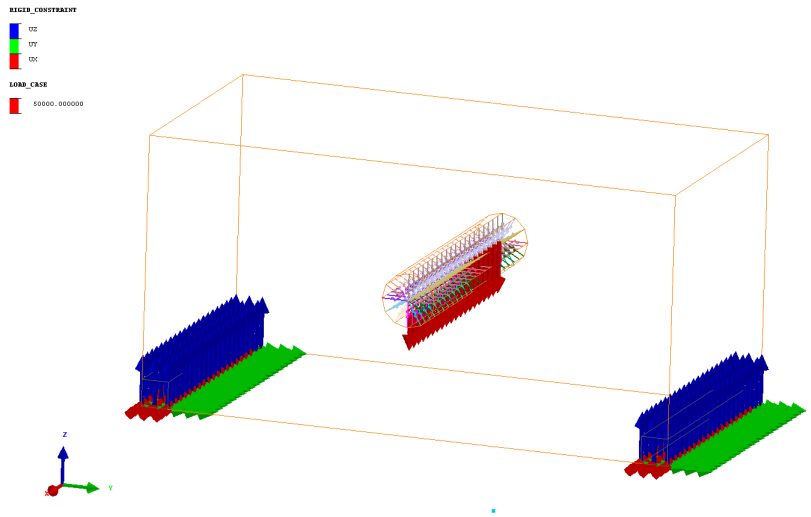

Figure 30: Load case for Example 17.

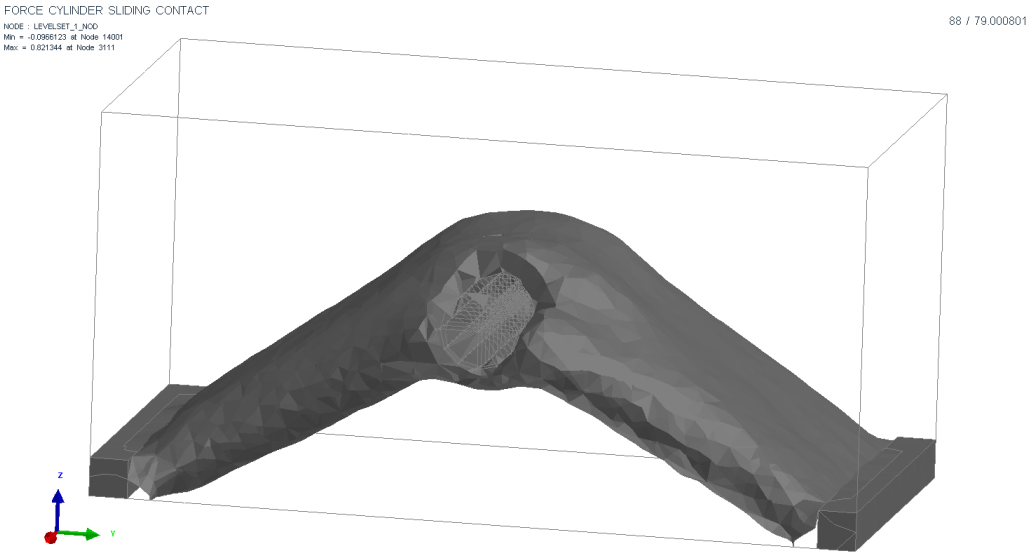

(a) Final design for frictionless contact

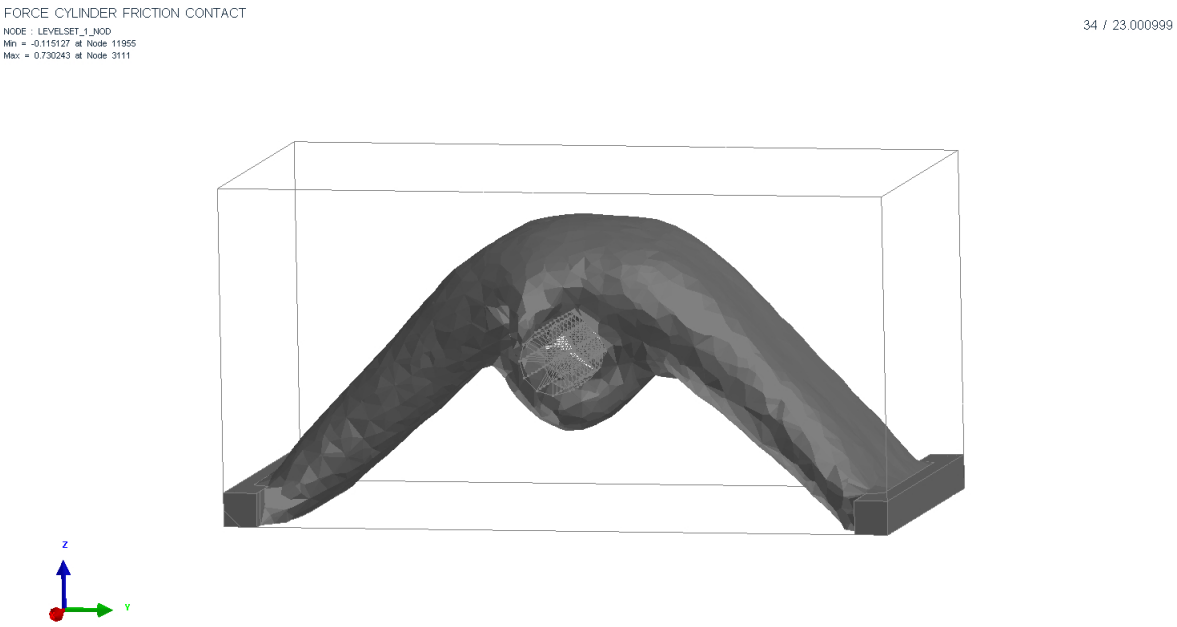

(b) Final design for the Tresca model

Figure 31: Example 17

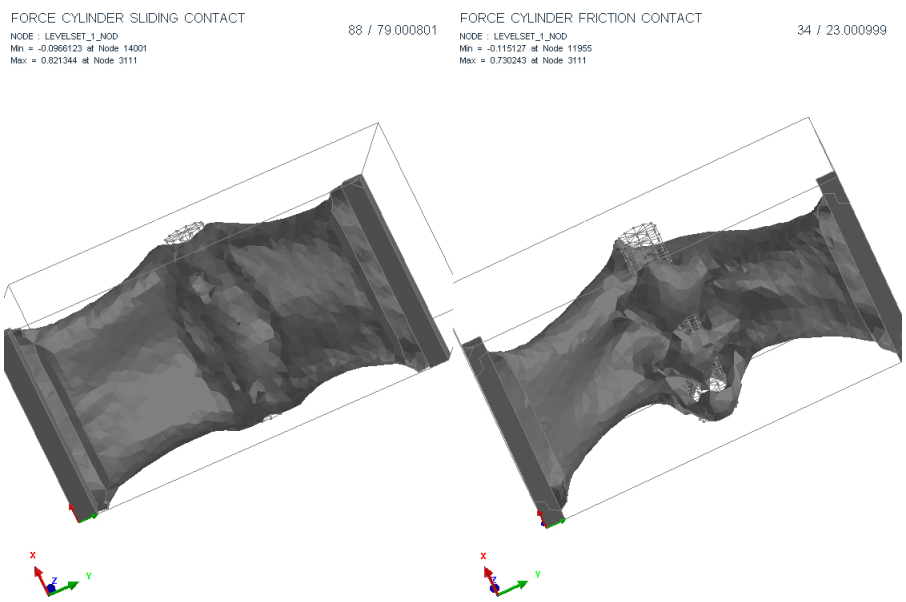

Figure 32: Comparison between without (left) and with (right) friction from below for Example 17

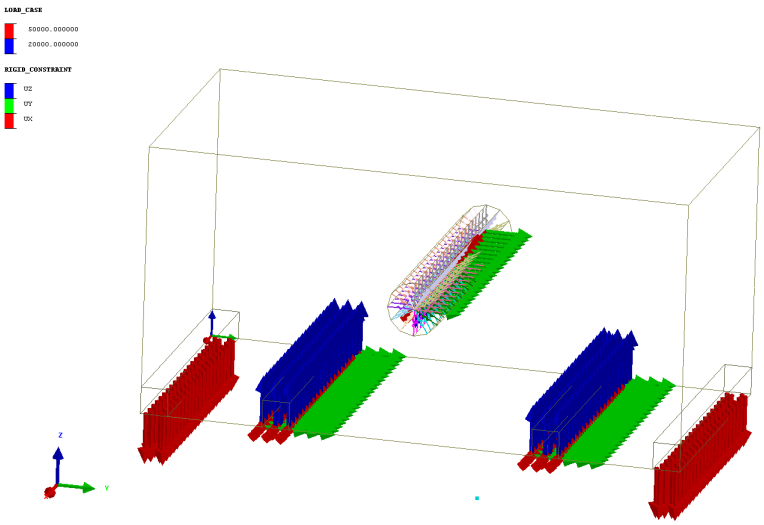

Figure 33: Load case for Example 18.

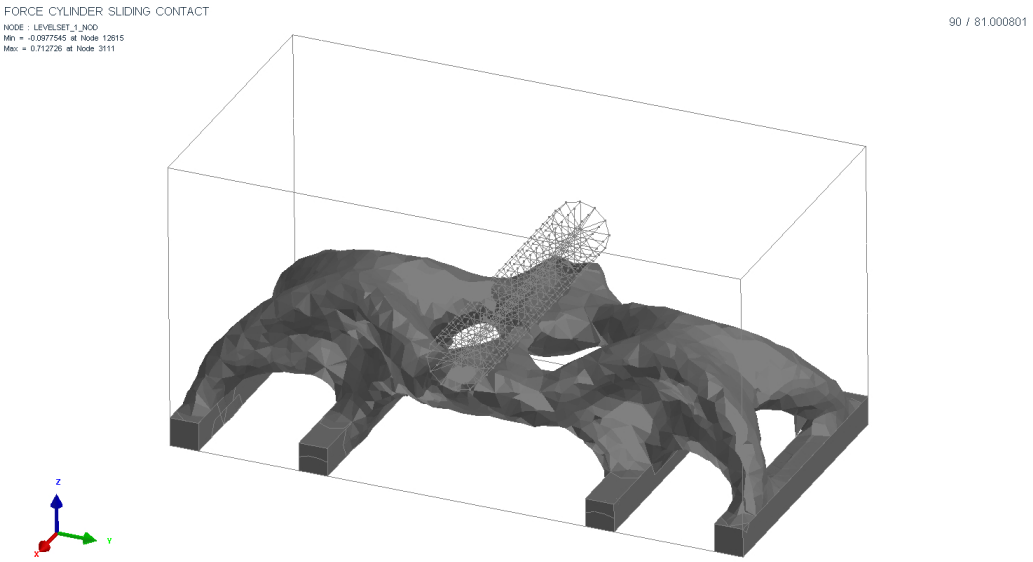

(a) Final design for frictionless contact

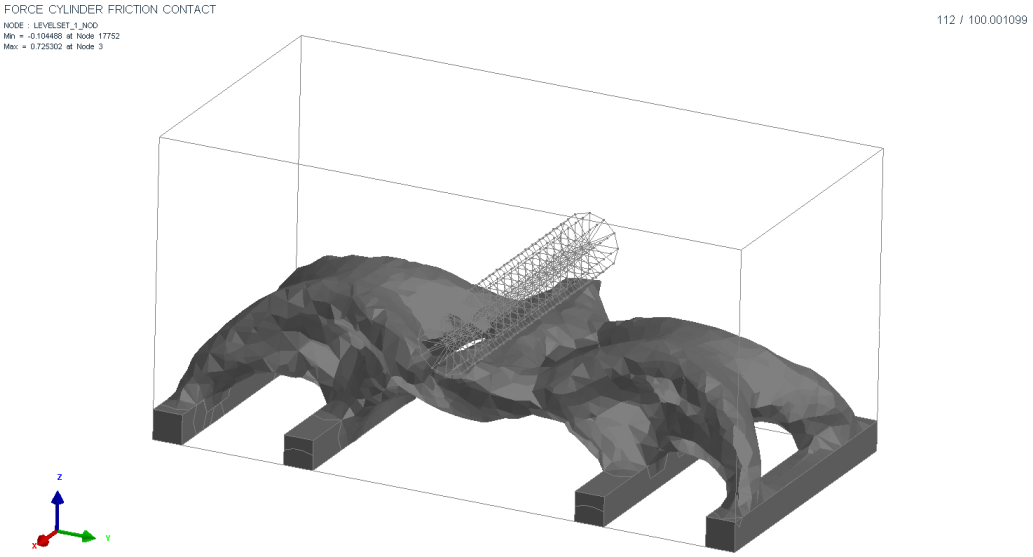

(b) Final design for the Tresca model

Figure 34: Example 18

References

[1] G. Allaire. *Conception optimale de structures*, volume 58 of *Mathématiques & Applications (Berlin) [Mathematics & Applications]*. Springer-Verlag, Berlin, 2007.

[2] G. Allaire, F. Jouve, and A.-M. Toader. Structural optimization by the level-set method. *International Series of Numerical Mathematics, Vol. 147*, pages 1–15, 2003.

[3] A. Amassad, D. Chenais, and C. Fabre. Optimal control of an elastic contact problem involving tresca friction law. *Nonlinear Analysis, 48*, pages 1107–1135, 2002.

[4] J. Andersson. Optimal regularity and free boundary regularity for the signorini problem. *St. Petersburg Mathematical Journal, Volume 24 (Number 3)*, pages 371–386, 2013.

[5] V. Barbu. *Optimal control of variational inequalities*, volume 100 of *Research Notes in Mathematics*. Pitman (Advanced Publishing Program), Boston, MA, 1984.

[6] P. Beremlijski, J. Haslinger, M. Kocvara, and J. Outrata. Shape optimization in contact problems with coulomb friction. *SIAM J. Optim Vol. 13, No 2*, pages 561–587, 2002.

[7] P. Beremlijski, J. Haslinger, J. Outrata, and R. Patho. Shape optimization in contact problems with coulomb friction and a solution-dependent friction coefficient. *SIAM J. Control Optim. Vol. 52, No 5*, pages 3371–3400, 2014.

[8] P. Boieri, F. Gastaldi, and D. Kinderlehrer. Existence, uniqueness, and regularity results for the two-body contact problem. *Appl. Math. Optim., 15*, pages 251–277, 1987.

[9] J. Cea. Conception optimale ou identification de formes, calcul rapide de la dérivée directionnelle de la fonction coût. *Modélisation mathématiques et analyse numérique 20-3*, pages 371–402, 1986.

[10] W.-H. Chen and C.-R. Ou. Shape optimization in contact problems with desired contact traction distribution on the specified contact surface. *Computational Mechanics 15*, pages 534–545, 1995.

[11] J. J. Dennis and R. Schnabel. *Numerical methods for unconstrained optimization and nonlinear equations*, volume 16 of *Classics in Applied Mathematics*. Society for Industrial and Applied Mathematics (SIAM), Philadelphia, PA, 1996. Corrected reprint of the 1983 original.

[12] B. Desmorat. Structural rigidity optimization with frictionless unilateral contact. *International Journal of Solids and Structures, Volume 44, Issues 3-4*, pages 1132–1144, 2007.

[13] S. Drabla, M. Sofonea, and B. Teniou. Analysis of a frictionless contact problem for elastic bodies. *Annales Polonici Mathematici*, 69(1):75–88, 1998.

[14] G. Duvaut and J. L. Lions. *Les inéquations en mécanique et en physique*, volume 21 of *Travaux et Recherches Mathématiques*. Dunod, Paris, 1972.

[15] C. Eck, J. Jarusek, and M. Krbec. *Unilateral contact problems, Variational methods and existence theorems*, volume 270 of *Pure and Applied Mathematics (Boca Raton)*. Chapman & Hall/CRC, Boca Raton, FL, 2005.

[16] ESI-group. *SYSTUS: a multiphysics simulation software*.

[17] R. Glowinski, J. L. Lions, and R. Trémolières. *Analyse numérique des inéquations variationnelles. Tome 1, Théorie générale premiéres applications*, volume 5 of *Méthodes Mathématiques de l'Informatique*. Dunod, Paris, 1976.

[18] H. Goldberg, W. Kampowsky, and F. Tröltzsch. On nemytskij operators in lp-spaces of abstract functions. *Mathematische Nachrichten*, 155(1):127–140, 1992.

[19] W. Han. On the numerical approximation of a frictional contact problem with normal compliance. *Numer. Funct. Anal. Optim., 17*, pages 307–321, 1996.

[20] J. Haslinger. Approximation of the signorini problem with friction, obeying coulomb law. *Math. Methods Appl. Sci., 5, No. 3*, pages 422–437, 1983.

[21] J. Haslinger. Shape optimization in contact problems. *Equadiff 6, Proceedings of the International Conference on Differential Equations and Their Applications*, pages 445–450, 1986.

[22] J. Haslinger. Signorini problem with coulomb law of friction. shape optimization in contact problems. *International Journal for Numerical methods in engineering, vol. 34*, pages 223–231, 1992.

[23] J. Haslinger and A. Klarbring. Shape optimization in unilateral contact problems using generalized reciprocal energy as objective functional. *Nonlinear Analysis, Theory, Methods and Applications, Vol. 21, No. 11*, pages 815–834, 1993.

[24] J. Haslinger and P. Neittaanmäki. On the existence of optimal shapes in contact problems. *Numer. funct. anal. and optimiz., 7(2 and 3)*, pages 107–124, 1985.

[25] J. Haslinger and P. Neittaanmäki. Shape optimization in contact problems. approximation and numerical realization. *Mathematical Modelling and Numerical Analysis, Vol. 21, No. 2*, pages 269–291, 1987.

[26] A. Henrot and M. Pierre. *Variation et optimisation de formes, une analyse géométrique. [A geometric analysis]*, volume 48 of *Mathématiques & Applications (Berlin) [Mathematics & Applications]*. Springer, Berlin, 2005.

[27] P. Hild. Two results on solution uniqueness and multiplicity for the linear elastic friction problem with normal compliance. *Nonlinear Analysis 71*, pages 5560–5571, 2009.

[28] D. Hilding, A. Klarbring, and J. Petersson. Optimization of structures in unilateral contact. *ASME Appl Mech Rev, vol 52, No 4*, pages 1–4, 1999.

[29] T. Iwai, A. Sugimoto, T. Aoyama, and H. Azegami. Shape optimization problem of elastic bodies for controlling contact pressure. *JSIAM Letters Vol.2*, pages 1–4, 2010.

[30] J. Jarušek and J. V. Outrata. On sharp necessary optimality conditions in control of contact problems with strings. *Nonlinear Analysis: Theory, Methods & Applications*, 67(4):1117–1128, 2007.

[31] N. Kim, K. Choi, and J. Chen. Shape design sensitivity analysis and optimization of elasto-plasticity with frictional contact. *AIAA Journal, Vol. 38, No. 9*, pages 1742–1753, 2000.

[32] N. Kim, K. Choi, J. Chen, and Y. Park. Meshless shape design sensitivity analysis and optimization for contact problem with friction. *Computational Mechanics 25*, pages 157–168, 2000.

[33] D. Kinderlehrer and G. Stampacchia. *An introduction to variational inequalities and their applications*, volume 88 of *Pure and Applied Mathematics*. Academic Press, Inc. [Harcourt Brace Jovanovich, Publishers], New York-London, 1980.

[34] A. Klarbring. On the problem of optimizing contact force distributions. *J. Optim. Theory Appl., Vol. 74, No 1*, pages 131–150, 1992.

[35] A. Klarbring, A. Mikelic, and M. Shillor. On friction problems with normal compliance. *Nonlinear analysis theory methods and applications, Vol 13, No 8*, pages 935–955, 1989.

[36] A. Klarbring, A. Mikelic, and M. Shillor. Optimal shape design in contact problems with normal compliance and friction. *Appl. Math. Lett. Vol.5, No 2*, pages 51–55, 1992.

[37] D. Knees and A. Schröder. Global spatial regularity for elasticity models with cracks, contact and other nonsmooth constraints. *Math. Meth. Appl. Sci., 35*, pages 1859–1884, 2012.

[38] P. Laborde and Y. Renard. Fixed point strategies for elastostatic frictional contact problems. *Math. Meth. Appl. Sci., 31*, pages 415–441, 2008.

[39] N. Mankame and G. Ananthasuresh. Topology optimization for synthesis of contact-aided compliant mechanisms using regularized contact modeling. *International Conference on Modeling, Simulation and Optimization for Design of Multi-disciplinary Engineering Systems 24-26 September, Goa, India*, 2004.

[40] J. Martins, J. Oden, and M. Shillor. Models and computational methods for dynamic friction phenomena. *Comput. Methods Appl. Mech. Engrg. 52*, pages 527–634, 1985.

[41] F. Mignot. Contrôle dans les inéquations variationelles elliptiques. *Journal of Functional Analysis*, 22(2):130–185, 1976.

[42] I. Milne, R. Ritchie, and B. Karihaloo. *Comprehensive structural integrity*. Elsevier Science, 2003.

[43] F. Murat and J. Simon. Etudes de problèmes d'optimal design. *Lecture Notes in Computer Science 41, Springer Verlag, Berlin*, pages 54–62, 1976.

[44] S. Osher and R. Fedkiw. *Level set methods and dynamic implicit surfaces*, volume 153 of *Applied Mathematical Sciences*. Springer-Verlag, New York, 2003.

[45] S. Osher and J. Sethian. Front propagating with curvature dependent speed: algorithms based on hamilton-jacobi formulations. *J. Comp. Phys., 78*, pages 12–49, 1988.

[46] J. Outrata. On the numerical solution of a class of stackelberg problems. *Methods and Models of Operations Research 34*, pages 255–277, 1990.

[47] J. Outrata, J. Jarušek, and J. Stará. On optimality conditions in control of elliptic variational inequalities. *Set-Valued and Variational Analysis*, 19(1):23–42, 2011.

[48] I. Paczelt and T. Szabo. Optimal shape design for contact problems. *Structural Optimization 7*, pages 66–75, 1994.

[49] O. Pironneau. *Optimal shape design for elliptic systems*. Springer Series in Computational Physics. Springer-Verlag, New York, 1984.

[50] R. Schumann. Regularity for signorini's problem in linear elasticity. *manuscripts math. 63*, pages 255–291, 1989.

[51] Scilab Enterprises. *Scilab: Le logiciel open source gratuit de calcul numérique*. Scilab Enterprises, Orsay, France, 2012.

[52] J. Sethian. *Level set methods and fast marching methods, Evolving interfaces in computational geometry, fluid mechanics, computer vision, and materials science*, volume 3 of *Cambridge Monographs on Applied and Computational Mathematics*. Cambridge University Press, Cambridge, second edition, 1999.

[53] J. Simon. Differentiation with respect to the domain in boundary value problems. *Num. Funct. Anal. Optimiz, 2*, pages 649–687, 1980.

[54] J. Sokolowski and J.-P. Zolesio. *Introduction to shape optimization, shape sensitivity analysis*, volume 16 of *Springer Series in Computational Mathematics*. Springer-Verlag, Berlin, 1992.

[55] N. Strömberg and A. Klarbring. Topology optimization of structures with contact constraints by using a smooth formulation and a nested approach. *8th Wolrd Congress on Strucutral and Multidisciplinary Optimization*, 2009.

[56] N. Strömberg and A. Klarbring. Topology optimization of structures in unilateral contact. *Struct Multidisc Optim, 41*, pages 57–64, 2010.

[57] S. Stupkiewicz, J. Lengiewicz, and J. Korelc. Sensitivity analysis for frictional contact problems in the augmented lagrangian formulation. *Computer Methods in Applied Mechanics and Engineering 199*, pages 2165–2176, 2010.

[58] N. Tardieu and A. Constantinescu. On the determination of elastic coefficients from indentation experiments. *Inverse Problems*, 16(3):577–588, 2000.

[59] F. Tröltzsch. *Optimal control of partial differential equations, Theory, methods and applications*, volume 112 of *Graduate Studies in Mathematics*. American Mathematical Society, Providence, RI, 2010.

[60] M. Y. Wang, X. Wang, and D. Guo. A level set method for structural topology optimization. *Computer methods in applied mechanics and engineering*, 192(1):227–246, 2003.